crystals

MDPI

Review

Development of Thermoelectric Half-Heusler Alloys over the Past 25 Years

Gerda Rogl * and Peter Franz Rogl

Institute of Materials Chemistry, University of Vienna, Währingerstraße 42, A-1090 Wien, Austria; peter.franz.rogl@univie.ac.at
* Correspondence: gerda.rogl@univie.ac.at

Abstract: Half-Heusler alloys are among the most promising thermoelectric materials. In the present review, thermoelectric properties (at 300 K and 800 K) of more than 1100 compositions from more than 220 publications between 1998 and 2023 were collected and evaluated. The dependence of the peak figure of merit, ZT_{max}, of p- and n-type half-Heusler alloys on the publishing year and the peak temperature is displayed in several figures. Furthermore, plots of *ZT* vs. the electrical resistivity, the Seebeck coefficient and the thermal conductivity at 300 K and 800 K are shown and discussed. Especially thermal conductivity vs. power factor leads to a good overview of *ZT*. For both p- and n-type individually separated into systems, *ZT*s and peak *ZT*s in dependence on the composition are displayed and discussed. This overview can help to find the ideal half-Heusler alloy for practical use.

Keywords: half-Heusler alloys; physical properties; figure of merit (*ZT*)

check for updates

Citation: Rogl, G.; Rogl, P.F. Development of Thermoelectric Half-Heusler Alloys over the Past 25 Years. *Crystals* **2023**, *13*, 1152. https://doi.org/10.3390/cryst13071152

Academic Editors: Bushra Jabar, Adil Mansoor and Jamil Ur Rahman

Received: 13 June 2023
Revised: 17 July 2023
Accepted: 19 July 2023
Published: 24 July 2023

1. Introduction

Thermoelectric (TE) modules and generators have the ability to directly convert waste heat into electric power and thus can be considered alternative, sustainable and "green" energy sources. There exist various classes of TE materials such as tellurides, selenides, clathrates, silicides, oxides, Zintl phases, antimonides, skutterudites, organic semiconductors, Heusler and half-Heusler alloys, etc., each of them qualifying in a defined temperature range. To judge the TE quality, the figure of merit, $ZT = S^2T/\rho(\lambda_e + \lambda_{ph})$, is used, where S is the Seebeck coefficient, ρ is the electrical resistivity, λ is the thermal conductivity, consisting of an electronic part, λ_e, and a phonon (lattice) part, λ_{ph}, and T is the temperature. To arrive at a high *ZT*, the power factor, $pf = S^2/\rho$, should be high, whereas λ should be low.

Half-Heusler (HH) alloys are promising TE materials intended for mid-to-high temperature power generation applications with already high *ZT* values. In addition, the starting materials are available, abundant, and, if hafnium and noble metals are avoided, cheap, a fact very important in respect of mass production.

Half-Heusler (HH) alloys are named after Friedrich Heusler (1866–1947), a German chemist and mining engineer. Half-Heusler alloys are members of the vast family of Heusler alloys with the general composition X_2YZ, consisting of three interpenetrating face-centered cubic (fcc) sublattices (space group $Fm\overline{3}m$). Reduction of symmetry (non-centrosymmetric space group F-43m) splits the X_2 sublattice of multiplicity eight into two sublattices of multiplicity four, of which one is empty, resulting in the formula XYZ of the so-called HH phases. The big advantage in the optimization of thermoelectric properties of HH compounds is the opportunity to dope each of the four sublattices individually. Besides that, HH alloys tend from metallic to half-metallic alloys, exhibit interesting magnetic properties and are small band gap semiconductors. Generally, one can divide HH alloys into the following main groups: MNiSn, MCoSb (M = Ti, Zr, Hf), MFeSb (M = V, Nb, Ta), the 19-electron system and other HH alloys not covered by these four systems.

Reviews as papers, chapters in a book, or even a book have been published [1–8] focusing mainly on the crystal structure, magneto-optical properties, electron–phonon interactions, mobility, ways to enhance the power factor, new advances, applications and so on. Freer et al. [9] recently published tables of TE materials: the chapter about HH alloys was handled by S. Han, C. Fu and T. Zhu. They collected TE parameters from about 90 publications of p- and n-type HH alloys, however, from each publication for the compound with the highest *ZT* only (for room temperature and the temperature of the peak *ZT*). These peak *ZT*s were also displayed as a figure.

In the current review, measured data of the Seebeck coefficient, the electrical resistivity and the thermal conductivity of all compositions in each published paper were collected, as well as the calculated power factor and *ZT* (at 300 K and 800 K) and particularly the peak *ZT*. As more than 220 papers were evaluated, this adds up to about 300 p-type and 810 n-type compositions. These data were plotted and evaluated to gain a deeper insight, e.g., *ZT* vs. Seebeck coefficient, resistivity, thermal conductivity, composition and pf vs. thermal conductivity.

2. Experimental Production Methods

There exist various methods to produce half-Heusler alloys, the basics of the most popular ones will be described as follows.

The historically favored route, and still the mostly used one, is the melting-annealing one. With some variations, the essential steps are to arc-melt the defined amounts of high-purity elemental pieces under argon, flip the reguli and remelt them several times for good homogenization. Oxygen contamination must be avoided; therefore, a certain vacuum level must be kept in combination with high-purity argon (the use of oxygen-getter material, such as Zr or Ti, which is melted prior to the actual samples, can further improve the sample quality). In some cases, the samples are additionally melted in a high-frequency induction furnace several times. Between the melting steps, it is possible to frequently break them into pieces and turn them upside down and outside-inside. As a last step, they are wrapped into protective Mo foils, vacuum sealed in a quartz ampulla and annealed at high temperatures, usually between 900–1000 °C for at least 48 h to equilibrate the samples and to further increase homogeneity.

This method is also suitable for big quantities (ingots with a weight of >1 kg) when stoichiometric amounts of pure elements are synthesized together in a vacuum induction furnace, and the melt is cast into a mold.

A similar production method is levitation melting (e.g., [10–12]), which is becoming more and more popular in recent years. The main advantage of levitation melting is that (i) the sample has no contact with the environment as well as (ii) the eddy currents, which improve the homogeneity of the melt.

All these above-described methods are followed by breaking the solidified samples and pulverizing them manually or, in recent years more often practiced, ball-mill (BM) or high-energy ball-mill (HBM) and consolidating them either via hot-pressing (HP) or spark plasma sintering (SPS). For half-Heusler alloys containing materials with a high vapor pressure at elevated temperatures, such as antimony, it is necessary to compensate for antimony vaporization losses before HP.

Mechanical alloying (MA) is a fast method (e.g., [13–16]) to prepare homogeneous powder mixtures prior to consolidation in HP or spark plasma sintering devices.

In the so-called solid-state reaction process (e.g., [17]), the powder mixture of high-purity constituents is heated (almost 1000 °C) under a flowing argon atmosphere for up to a week, usually followed by SPS.

Self-propagation high-temperature synthesis (SHS) or combustion synthesis (CS) is a scalable, rapid preparation method. It is based on a propagating self-sustained exothermic reaction in consolidated elemental powders of the desired composition, and it yields a homogeneous product similar to the ones obtained by the well-known zone melting process. In addition, the SHS process is so fast that evaporation of low-melting-point elements is

dramatically suppressed, leading to a precisely controlled composition (for details, see, e.g., [18–20]).

In some cases, SHS is combined with the selective laser melting (SLM) method. For SLM, a laser beam is used to melt a single-layer powder bed that rapidly solidifies as soon as the laser moves away. Layer upon layer, a three-dimensional object can be formed.

Microwave preparation (e.g., [21–24]) is another fast way to prepare half-Heusler alloys. Stoichiometric amounts of metal powders are cold-pressed into bar-shaped pellets, directly sealed into evacuated quartz tubes and placed into a crucible filled with some granular carbon, which acts as the microwave susceptor material. The sample is surrounded by alumina insulation foam to minimize heat loss. Finally, the whole set-up is placed into a commercial microwave reactor with a rotating plate. The reactions are allowed to run at 100% power (e.g., 700 W) for 1 min.

In some cases, the bulk HH alloy is processed by high-pressure torsion to further improve the TE performance by severe plastic deformation resulting in a drastic reduction towards ultra-low thermal conductivity, which occurs due to grain refinement and deformation-induced defects (for details, see references [25–27]).

Whenever the phonon part of the thermal conductivity was not published, it was calculated by the authors: $\lambda_{ph} = \lambda - \lambda_e$ with λ as the total thermal conductivity and λ_e as the electron part; $\lambda_e = LT/\rho$ (Wiedemann–Franz law) with L as the Lorenz number (calculated as suggested by Kim et al. [28]) and ρ is the electrical resistivity. In all cases where the power factor and/or *ZT* were not published, it was calculated by the authors from $pf = S^2/\rho$ and $ZT = S^2T/(\rho\lambda)$, respectively.

3. Results and Discussion

3.1. General Overview

In this chapter, all data from references [10–27,29–218] were used for figures and discussions. The references [29–218] are numbered by the publication year, within one year, in alphabetical order.

Looking at the highest *ZT*s published during the last 25 years, one can see in Figure 1 that, as already mentioned in the introduction, considerably more n-type half-Heusler alloys were investigated than p-type (this review comprises 294 p-type compounds and 816 n-type compounds). It is also clearly visible that the trend of high peak *ZT*s increases almost linearly from 2004 to 2018. There are exceptions for the n-type, such as (i) the work of Sakurada et al. [43], who published already in 2005 outstanding high values (ZT = 1.25 to 1.5) for $Ti_{0.5}Zr_{0.25}Hf_{0.25}NiSn$ doped with small amounts of antimony, or (ii) from Shen et al. [17,33] and Kawasaki et al. [37], who reached almost *ZT*s = 1 at 800 K in 2001 and 2004 for $ZrNiSn_{0.99}Sb_{0.01}$. It is also worth mentioning that Yu et al. [150] reached ZT = 1.6 at 1200 K for his p-type HH series $(Nb_{1-x}Ta_x)_{0.8}Ti_{0.2}FeSb$. Furthermore, it seems that after a boom during 2015–2020, the number of half-Heusler publications has dropped significantly.

Figure 2 displays the highest *ZT*s as a function of temperature. It is necessary to point out that in some cases ZT_{max} is not really the peak ZT of the respective sample but the ZT at the highest measured temperature. This is especially the case for publications earlier than 2005. Besides that, in most cases ZT_{max} is published for temperatures between 700 K and 1000 K; the highest temperatures for ZT_{max} for p- as well as n-type are around 1200 K.

Figures 3 and 4 depict the dependence of the power factor on the thermal conductivity at 300 K and 800 K, respectively. Figure 3 shows that at 300 K, almost all power factor values for the n-type are within the range of 4 mW/mK^2 for thermal conductivities up to 250 mW/cmK, whereas the p-type displays much higher power factors, reaching values higher than 10 mW/mK^2 for thermal conductivities up to about 150 mW/cmK, e.g., for the $Nb_{1-x}Ti_xFeSb$-series of He et al. [131] or for $Nb_{0.95}Hf_{0.05}FeSb$ and $Nb_{0.95}Zr_{0.05}FeSb$ of Ren and colleagues [160].

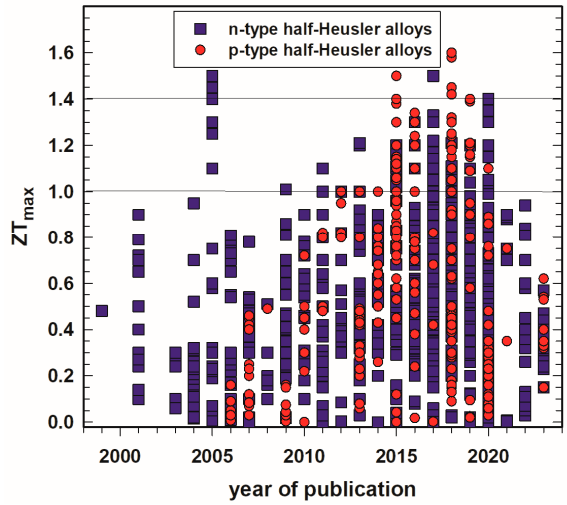

Figure 1. Peak ZT, ZT_{max}, of p- and n-type half-Heusler alloys vs. year of publication.

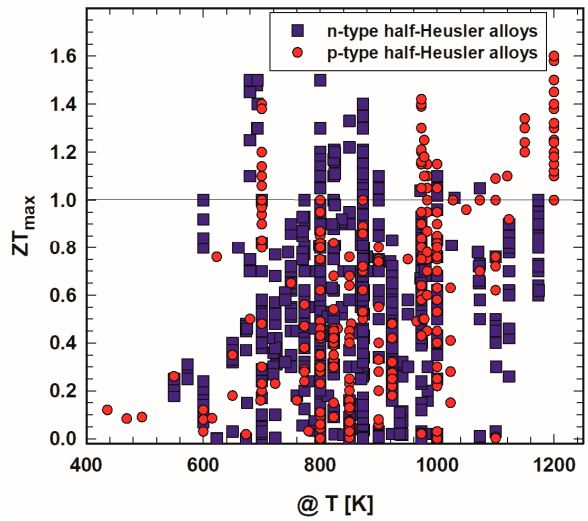

Figure 2. Peak ZT, ZT_{max}, of p- and n-type half-Heusler alloys vs. temperature, T.

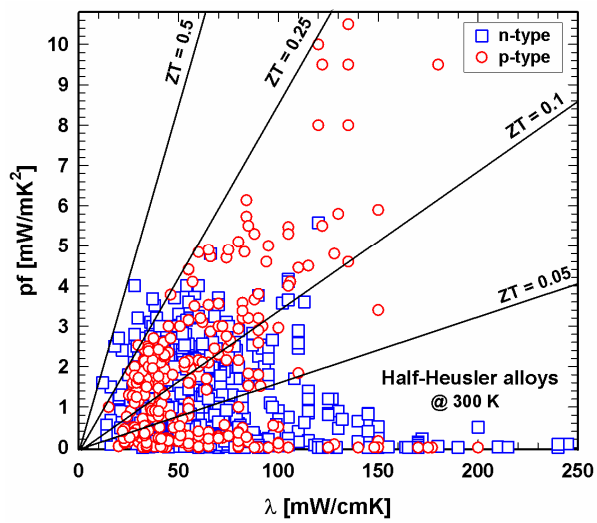

Figure 3. P- and n-type half-Heusler alloys: power factor, pf, vs. thermal conductivity, λ, at 300 K.

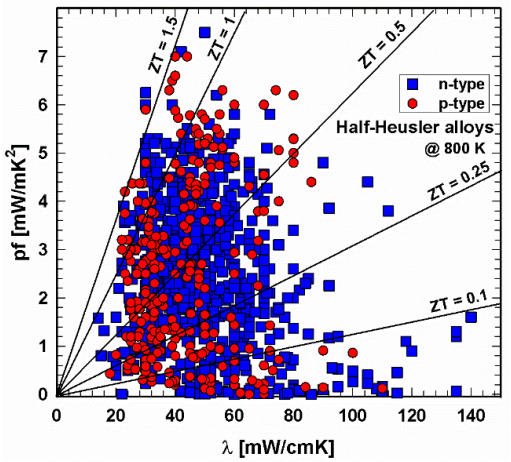

Figure 4. P- and n-type half-Heusler alloys: power factor, pf, vs. thermal conductivity, λ, at 800 K.

The situation has changed comparing this figure now with the one for 800 K (Figure 4), and as for p- and n-type, all data are mainly evenly distributed within a power factor–thermal conductivity window of almost 0–5.5 mW/mK^2 by 20–80 mW/cmK.

Lines for the resulting *ZT* values are drawn in both Figures 3 and 4, revealing that at 300 K, no compound exceeds *ZT* = 0.5. Whilst many of the p-type compounds range between *ZT* = 0.1 and 0.25 or have values as low as almost 0, one can find the values for the n-type all over, the very low values due to high thermal conductivities. At 800 K, both p- and n-type exceed the *ZT* = 1.5 line. The majority of data can be found for thermal conductivities between 20 and 80 mW/cmK, representing *ZT*s from almost 0 to *ZT* = 1.5. This figure also illustrates that p-type HH materials generally exhibit lower thermal conductivities than the n-type.

Figures 5 and 6 depict the relation between electrical resistivity and *ZT* at 300 K and 800 K, respectively. It shows that, especially in the 300 K temperature region, individual specimens have very high resistivities, resulting, as a consequence, in very low *ZT*s. Generally, the electrical resistivity decreases with increasing temperature. Figure 6 displays lower resistivity values. Still, here one can find *ZT*s in the range of 10^{-3} or even lower. The insert, a cutout, in each *ZT*-resistivity figure, gives a better overview, indicating that, especially for 800 K, most data can be found between 500 and 2500 μΩcm. In this region are also the highest *ZT*s.

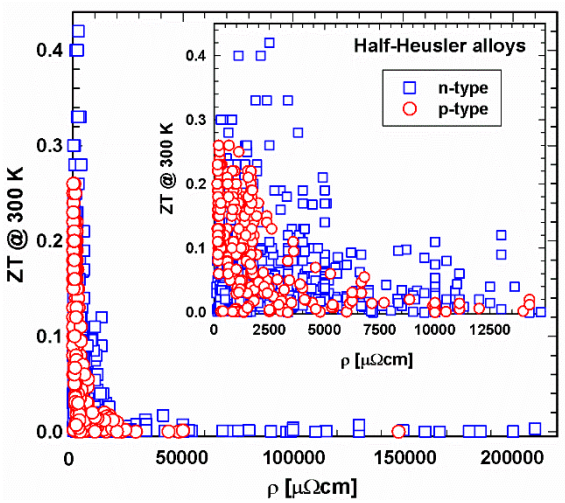

Figure 5. *ZT* at 300 K vs. electrical resistivity, ρ, for p- and n-type half-Heusler alloys. Insert: cutout for ρ < 15000 μΩcm.

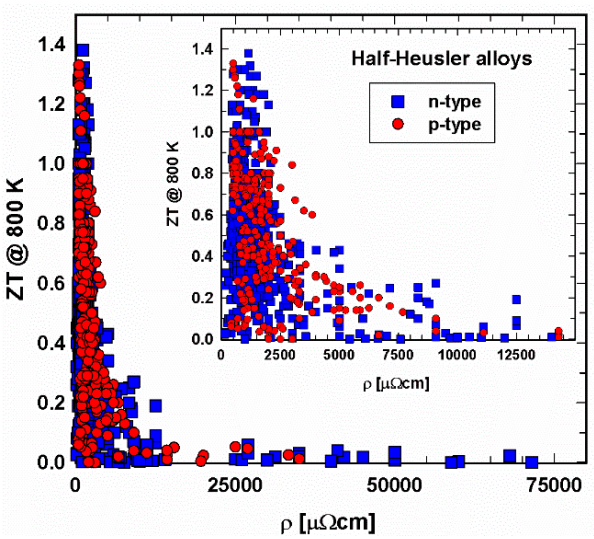

Figure 6. *ZT* at 800 K vs. electrical resistivity, ρ, for p- and n-type half-Heusler alloys. Insert: cutout for ρ < 12000 μΩcm.

Figures 7 and 8 present the dependence of *ZT* on the Seebeck coefficient. Especially at 300 K, the area of Seebeck values is much wider for the n- than for the p-type. Generally, it seems that an absolute Seebeck value of 200 ± 20 μV/cm leads to high *ZT*s, a great finding for the production of new half-Heuslers.

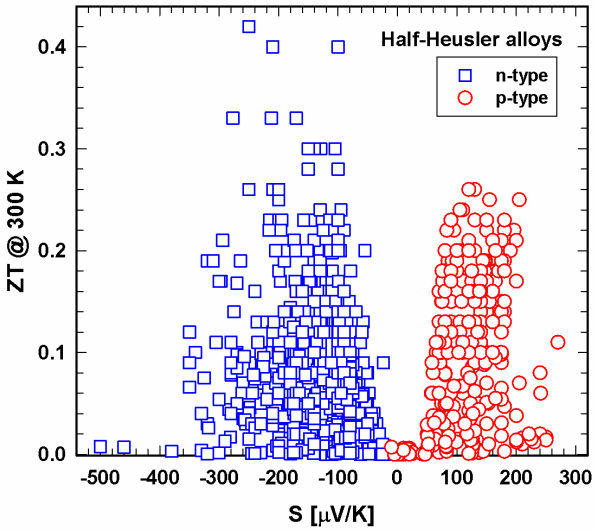

Figure 7. *ZT* at 300 K vs. Seebeck coefficient, S, for p- and n-type half-Heusler alloys.

Whereas for the high-temperature regime (Figure 9), the data *ZT* vs. λ are more or less evenly mixed at 300 K (insert in Figure 9), most p-type half-Heuslers have thermal conductivities between 20 and 70 mW/cmK. Of course, in both regions, *ZT*s are high for low thermal conductivities. Comparing the total and the lattice thermal conductivities in Figures 9 and 10, the distribution of the data looks very similar, indicating that the electron part of the thermal conductivity is rather low, and, as a consequence, the phonon part is in the range of the total thermal conductivity.

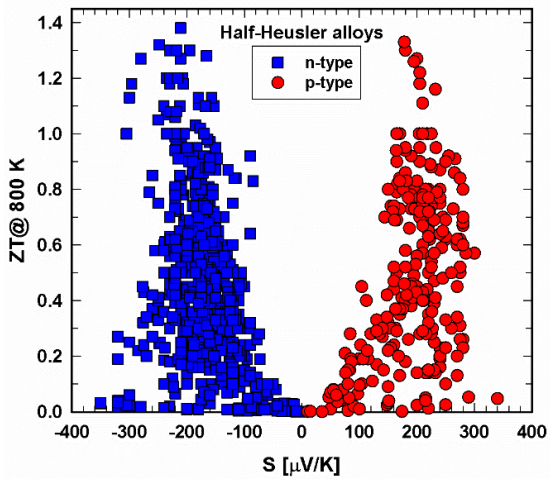

Figure 8. *ZT* at 800 K vs. Seebeck coefficient, S, for p- and n-type half-Heusler alloys.

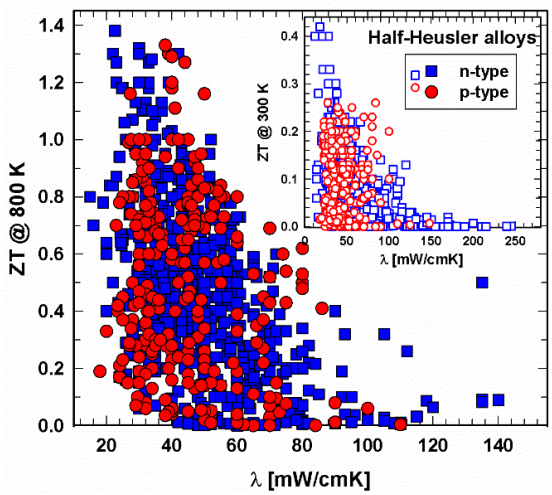

Figure 9. *ZT* at 800 K vs. thermal conductivity, λ, for p- and n-type half-Heusler alloys. Insert: *ZT* at 300 K vs. thermal conductivity, λ.

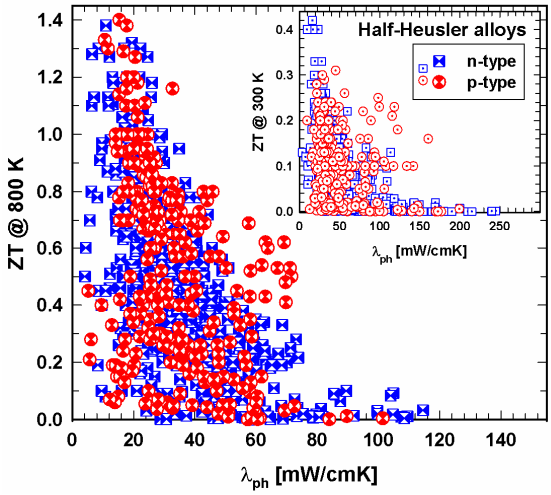

Figure 10. *ZT* at 800 K vs. lattice thermal conductivity, λ_{ph}, for p- and n-type half-Heusler alloys. Insert: *ZT* at 300 K vs. lattice thermal conductivity, λ_{ph}.

In this chapter, it was only distinguished between p- and n-type half-Heusler alloys. In the following paragraphs for p- and n-type half-Heusler alloys, in addition, the various sys-

tems, i.e., the (Ti,Zr,Hf)NiSn-system, the (Ti,Zr,Hf)CoSb-system, the (V,Nb,Ta)FeSb-system, the 19-electron system and other p- and n-type HH materials (see also Tables 1 and 2) will be discussed separately.

Table 1. N-type half-Heusler alloys.

N-Type Half-Heusler Alloys (Ti,Zr,Hf)NiSn-System	X	Z	References (Marked with *: Not Measured above RT)
TiNiSn			[19,21–23], [31] *, [30,34,39,58,75,83,88,90,99,139,143,144,152,178,210,213]
TiNiSn/Z		Sb	[24,39,58]
		Si	[34]
(Ti,X)NiSn	Nb		[66]
	Ta		[178,212]
Ti(Ni,X)Sn	Mn		[138,139,144]
	Pd		[17]
	Pt		[34]
	Cu		[152]
Ti(Ni,X)Sn/Z	Co	Sb	[48,67,179,198,207,208]
ZrNiSn			[6,7,10,12,14,17], [29,31,32] *, [33,35–37,42,57,66,70,71,85,99,106,108,110,119,122,123,129,153–155,166,171,174,196,203,210,212]
ZrNiSn/Z		In	[32] *
		Si	[181]
		Ge	[181,196]
		Sb	[10,17,19], [32] *, [37,123,195]
		Bi	[145]
(Zr,X)NiSn	Sc		[122]
	Y		[57,114]
	V		[155]
	Nb		[66]
	Ta		[203,212]
Zr(Ni,X)Sn	Pd		[33,34]
	Cu		[36]
	Co + Cu		[36]
Zr(Ni,X)Sn/Z	Pd	Sb	[33]
HfNiSn			[12], [31] *, [99,119,129,195]
HfNiSn/Z		Sb	[129]
(Ti,Zr)NiSn			[25–27,31,34,65,69,90,99,100,129,161]
(Ti,Zr)NiSn/Z		Sb	[25–27,90,99,100,149,161,201,210]
(Ti,Zr,X)NiSn/Z	V	Sb	[146]
	Nb	Sb	[146]
(Ti,Hf)NiSn			[31] *, [34,58,65,69,90,102,124,129,134,143]
(Ti,Hf)NiSn/Z		Sb	[58,143]
(Ti,Hf,X)NiSn	Nb		[31] *
(Ti,Hf)(Ni,X)Sn	Pd		[58]

Table 1. *Cont.*

N-Type Half-Heusler Alloys (Ti,Zr,Hf)NiSn-System	X	Z	References (Marked with *: Not Measured above RT)
(Zr,Hf)NiSn			[11], [31,32] *, [65,77,78,80,81,84,87,90,93,99,109,137,154,156,190]
(Zr,Hf)NiSn/Z		Sb	[11,12,18,43,49,50,73,76,77,79,89,93,95,98,111,119,124,127,129,132,133,135,138,140,146,172,187,201,204]
(Zr,Hf,X)NiSn	V		[81]
	Nb		[31] *
	Ta		[203,212]
(Zr,Hf)(Ni,X)Sn	Pd		[17], [29] *, [33,49,50]
	Pt		[95]
(Zr,Hf,X)NiSn/Z	Y	Sb	[73]
	V	Sb	[140]
	Nb	Sb	[137,140]
	Ta	Sb	[140]
(Zr,Hf)(Ni,X)Sn/Z	Pd	Sb	[33]
(Ti,Zr,Hf)NiSn			[40,41,43,47], [49] *, [105,129,146,170,183]
(Ti,Zr,Hf)NiSn/Z		Sb	[43,127,189]
		Bi	[77,93]
		Te	[93]
(Ti,Zr,Hf,X)NiSn	Nb		[105]
(Ti,Zr,Hf)(Ni,X)Sn	Cu		[170]
(Ti,Zr,Hf,X)NiSn/Z	V + Nb	Sb	[174]
(Ti,Zr)$Ni_{1\pm x}$Sn			[22,110,171]
(Ti,Zr)$Ni_{1\pm x}$Sn			[138]
(Zr,Hf)$Ni_{1\pm x}$Sn			[77]
TiNiSn+full Heusler			[83]
TiNiSn+HfO_2			[149]
ZrNiSn+B			[29] *
ZrNiSn+La			[108]
ZrNiSn+ZrO_2			[35]
ZrNiSn+ZnO			[153]
(Zr,Hf)NiSn+W			[197]
(Zr,Hf)NiSn+ZrO_2			[95]
(Zr,Hf)NiSn/Z+Nb		Sb	[80] *
(Zr,Hf)NiSn/Z+full Heusler		Sb	[77,78]
(Zr,Hf)(Ni,X)Sn/Z+ZrO_2	Pd	Sb	[49]
(Ti,Zr,Hf)NiSn/Z+ZrO_2		Sb	[17]
(Ti,Zr,Hf)CoSb-System			
TiCoSb			[38,44,46,48,55,56,61,68,177]
(Ti,X)CoSb	Ta		[204]
Ti(Co,X)Sb	Fe		[61]
	Ni		[48]

Table 1. *Cont.*

N-Type Half-Heusler Alloys (Ti,Zr,Hf)NiSn-System	X	Z	References (Marked with *: Not Measured above RT)
(Ti,X)CoSb/Z	Nb + Ta	Sn	[38]
ZrCoSb			[3,45,46,56,60,141,147,177]
(Zr,X)CoSb	Nb		[156]
Zr(Co,X)Sb	Ni		[141]
HfCoSb			[45,46,56,177,195]
(Hf,X)CoSb	Nb		[182]
(Ti,Zr)CoSb			[67]
(Ti,Zr)(Co,X)Sb	Ni		[67]
(Ti,Hf,X)CoSb	Ta		[204]
(Zr,Hf,X)CoSb	Nb		[158,182]
	Nb + Ta		[214]
(Ti,Zr,Hf)CoSb			[56,64]
(Ti,Zr,Hf)(Co,X)Sb	Ni		[64]
(V,Nb,Ta)FeSb-System			
VFeSb			[74,91,192]
(V,X)FeSb	Ti		[15]
NbFeSb			[26,148]
Nb(Fe,X)Sb	Ir		[184]
(V,Nb)FeSb			[92]
(V,Nb)(Fe,X)Sb	Co		[92]
Ti(Fe,X)Sb	Ni		[200]
Ti(Fe,X)Sb/Z	Ni	Sn	[13]
19-Electron System			
VCoSb			[136,173,176,199]
VCoSb/Z		Sn	[136]
NbCoSb			[116,117,142,151,165,173]
Nb(Co,X)Sb	Ni		[186]
NbCoSb/Z		Sn	[142]
TaCoSb			[173]
(Ti,V)CoSb			[136,199]
(V,Nb)CoSb			[117]
(Nb,Ta)CoSb			[117]
(V,Nb,Ta)CoSb			[117]
(Ti,Nb,Ta)CoSb/Z		Sn	[38]
TiNiSb			[212]
(Ti,X)NiSb	Sc		[212]
TiPtSn			[194]
Other N-type Half-Heusler Material			
TiCoSn			[21]

Table 1. *Cont.*

N-Type Half-Heusler Alloys (Ti,Zr,Hf)NiSn-System	X	Z	References (Marked with *: Not Measured above RT)
TiPtSn			[51]
VCoSn			[207]
NbCoSn			[130,180,202]
NbCoSn/Z		Sb	[52,63]
Nb(Co,X)Sn	Pt		[202]
(Nb,Ti)Sn/Z		Sb	[52]
TaCoSn			[180]
(Ta,X)CoSn	Nb		[180]
(Ta,X)CoSn/Z	Nb	Sb	[180]
ZrCoBi			[167,187]

Table 2. P-type half-Heusler alloys.

P-Type Half-Heusler Alloys (Ti,Zr,Hf)NiSn-System	X	Z	References
(Zr,X)NiSn	Sc		[122]
	Y		[114]
ZrNiSn + Co			[71]
ZrNiSn + Ir			[71]
(Ti,Zr,Hf)CoSb-System			
TiCoSb			[54,211]
TiCoSb/Z		Ge	[68]
TiCoSb/Z		Sn	[55,107,120,164]
ZrCoSb/Z		Sn	[16,19,60,107,126]
HfCoSb/Z		Sn	[107,120]
(Ti.Zr)CoSb/Z		Sn	[107]
(Ti,Hf)CoSb/Z		Sn	[18,86,107,120,121,132,159]
(Zr,Hf)CoSb/Z		Sn	[62,76,82,98,107,115,132,156,157]
(Ti,Zr,Hf)CoSb/Z		Sn	[96,107,121]
(Ti,Hf)CoSb/Z+$Cu_{1.96}Ni_{0.04}Te_{0.97}Se_{0.03}$		Sn	[159]
(Zr,Hf)CoSb/Z+HfO_2		Sn	[103]
(Ti,Zr)[Fe,(Fe,Co),(Fe,Ni)]Sb-System			
TiFeSb			[164]
Ti(Fe,Co)Sb			[61,94,164,206,218]
Ti(Fe,Co)Sb/Z		Sn	[164]
(Ti,Zr)(Co,Fe)Sb			[218]
(Ti,Zr)(Co,Fe)Sb/Z		Sn	[218]
Ti(Fe,Ni)Sb			[200]
Ti(Co,Fe)Sb+InSb			[94]

Table 2. *Cont.*

P-Type Half-Heusler Alloys (Ti,Zr,Hf)NiSn-System	X	Z	References
(V,Nb,Ta)FeSb-System			
(V,X)FeSb	Ti		[15,97]
	Hf		[192]
	Ti + Hf		[193]
NbFeSb			[27,112,131,147,195,206]
(Nb,X)FeSb	Ti		[104,112,128,131,148,160,163,183,201,206]
	Zr		[113,148,160,163]
	Hf		[113,148,160,163,168]
	Ti + Hf		[26,162]
	Ti + Ta		[150,204]
(V,Nb,X)FeSb	Ti		[101,112]
TaFeSb			[175,188]
(Ta,X)FeSb	Ti		[175,188]
Other P-Type Half-Heusler Material			
NbCoSb/Z		Sn	[201]
ZrCoBi/Z		Sn	[169]
ZrPtSn			[51]
HfPtSn			[51]
ScNiSb			[185,191]
DyNiSb			[191]
ErNiSb			[191]
TmNiSb			[191,212]
LuNiSb			[191]
YNiBi			[118]
ErPdSb			[53]
ErPdBi			[53]
LaPdBi			[59]
GdPdBi			[59]

3.2. N-Type Half-Heusler Alloys

All compounds with the respective references can be found in Table 1. In some cases (indicated by *), measurements were only performed below room temperature.

3.2.1. (Ti,Zr,Hf)NiSn-System

Comparing the *ZT* values of TiNiSn, ZrNiSn and HfNiSn, as shown in Figures 11 and 12, one can immediately see that ZrNiSn is the most investigated alloy of these three, whereas HfNiSn is not so popular. It is evident from Figures 11 and 12 that the highest *ZT*s at 300 K as well as at 800 K in this system are for (Zr,Hf)NiSn and (Ti,Zr,Hf)NiSn and even more so when Sb-doped at the Sn site.

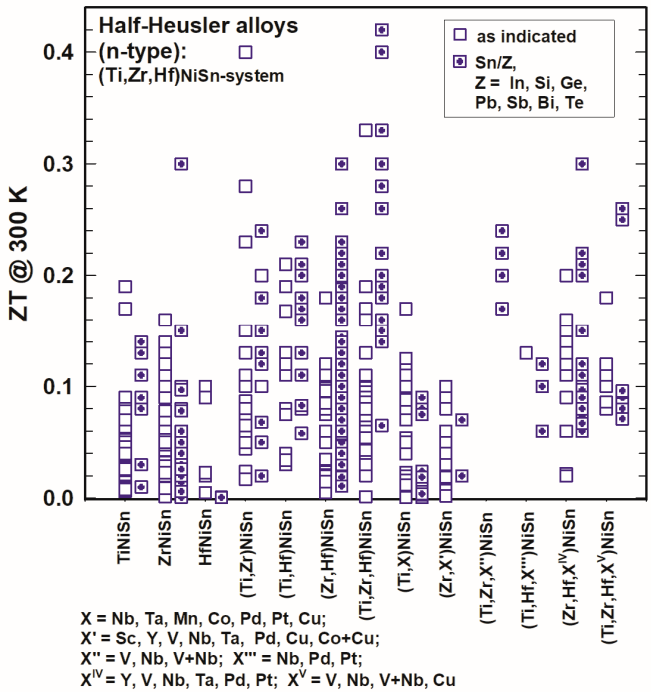

Figure 11. *ZT* at 300 K for the HH n-type (Ti,Zr,Hf)NiSn-system.

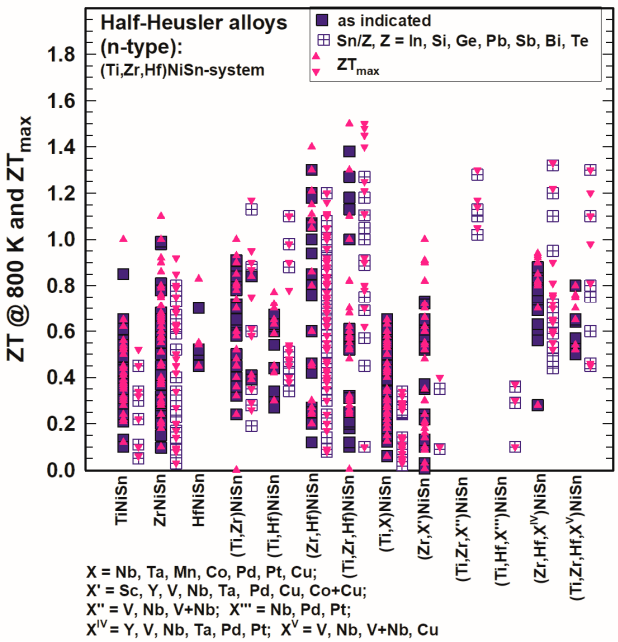

Figure 12. *ZT* at 800 K and ZT_{max} for the HH n-type (Ti,Zr,Hf)NiSn-system.

Gürth et al. [129] published *ZT* = 1 at 823 K for TiNiSn and for ZrNiSn, Misra et al. [106] *ZT* = 0.9 at 773 K for ZrNiSn and Liu et al. [119] *ZT* = 0.8 at 1000 K for HfNiSn. In comparison to these values, those for compounds with Ti and Zr, Ti and Hf, Zr and Hf or with Ti and Zr and Hf reach much higher values, such as for $Zr_{0.7}Hf_{0.3}NiSn$ *ZT* = 1.2 at 873 K (Chauhan et al. [154]), for $Ti_{0.5}Zr_{0.25}Hf_{0.25}NiSn$ *ZT* = 1.3 at 693 K (Sakurada and Shutoh [43]; Shutoh and Sakurada [47]) or even *ZT* = 1.5 at 800 K (Rogl et al. [146]).

Doping in the (Ti,Zr,Hf)NiSn-system with X (X = Sc, Y, V, Nb, V + Nb, Ta, Mn, Co, Cu, Co + Cu, Pd, Pt, Pb) (see also Table 1) was not really successful as generally, all these alloys did not have higher *ZT*s; however, from Figure 11 as well as from Figure 12 it is obvious that with an additional substitution of Sn in many cases *ZT* is enhanced. Usually, Sn is substituted by a very small amount of Sb or Ge, but also, in rarer cases, In, Si, Pb, Bi or Te was used. The highest *ZT* values were reached for $Ti_{0.5}Zr_{0.25}Hf_{0.25}NiSn_{0.998}Sb_{0.002}$ at 700 K (*ZT* = 1.5, Shutoh and Sakurada [47]) and $Ti_{0.5}Zr_{0.25}Hf_{0.25}NiSn_{0.99}Sb_{0.01}$ at 825 K (*ZT* = 1.45, Rogl et al. [146]). Besides that, there are several compounds with $ZT \sim 1.3$, such as $(Hf_{0.6}Zr_{0.4})_{0.99}V_{0.01}NiSn_{0.995}Sb_{0.005}$ at 900 K (Chen et al. [140]) or $Ti_{0.49}Zr_{0.49}V_{0.02}NiSn_{0.98}Sb_{0.02}$ at 823 K (Rogl et al. [146]) (see also Figure 12).

Various groups used additions (not shown in any figure but presented in Table 1), mainly nanoparticles, to reduce the thermal conductivity and to enhance *ZT*. Schwall and Balke [80] incorporated Nb into $Zr_{0.5}Hf_{0.5}NiSn$ but presented data only below room temperature. Akram et al. [108] admixed La with ZrNiSn: the enhancement in *ZT* was within the error bar of *ZT* (from 0.52 to 0.54), which also applies to Visconti et al. [149], who used HfO_2 for $Ti_{0.5}Zr_{0.5}NiSn_{0.994}Sb_{0.006}$ (*ZT* rises from 0.9 to 1). A better result was achieved by Chauhan et al. [153] by mixing ZnO with ZrNiSn (highest *ZT* = 1). Nanoparticles of ZrO_2 were added to ZrNiSn (Huang et al. [35]) as well as to $Zr_{0.5}Hf_{0.5}Ni_{0.8}Pd_{0.2}Sn_{0.99}Sb_{0.01}$ and $Zr_{0.25}Hf_{0.6}Ti_{0.15}NiSn_{0.995}Sb_{0.005}$ (Chen et al. [49] and [127], respectively). For ZrNiSn, the "enhancement" of *ZT* was within the error bar; however, it was much better for the other two compounds with ZT_{max} = 0.74 and even ZT_{max} = 1.3 for the Ti-doped half-Heusler alloy. Additionally, a rather high ZT_{max} = 1.35 at 873 K was achieved by Kang et al. [197] for $Zr_{0.4}Hf_{0.6}NiSn_{0.99}Sb_{0.01}$ plus 2 weight percent tungsten nanoparticles. Makongo et al. [77,78] and Douglas et al. [83] added to $Zr_{0.25}Hf_{0.75}NiSn$ and TiNiSn the corresponding full Heusler phase, i.e., $Zr_{0.25}Hf_{0.75}Ni_2Sn$ and $TiNi_2Sn$, respectively; however, the outcome was rather disappointing with low *ZT*s < 1, in some cases even lower than *ZT* without the full-Heusler phase.

Rogl et al. [25,26] processed arc-melted, annealed, ball-milled and hot-pressed $Ti_{0.5}Zr_{0.5}NiSn$ and $Ti_{0.5}Zr_{0.5}NiSn_{0.98}Sb_{0.02}$ samples by high-pressure torsion to improve their thermoelectric performance via a drastic reduction of the thermal conductivity due to grain refinement and a high concentration of defects inferred by severe plastic deformation. Whereas for $Ti_{0.5}Zr_{0.5}NiSn$, the thermally stable alloy showed an enhancement of ZT_{max} of 20%, for $Ti_{0.5}Zr_{0.5}NiSn_{0.98}Sb_{0.02}$ ZT_{max} was, within the error bar, about the same.

As a summary, one can say that the (Ti,Zr,Hf)NiSn-system comprises TE materials of high interest.

3.2.2. (Ti,Zr,Hf)CoSb-System, (V,Nb,Ta)FeSb-System, 19-Electron System and Other N-Type Half-Heusler Alloys

In Figures 13 and 14, the *ZT*s are shown for the (Ti,Zr,Hf)CoSb-system, the (V,Nb,Ta)FeSb-system, the 19-electron system and of all those half-Heuslers, which do not fit into any of the so-far mentioned categories. For all these systems, only a few half-Heuslers with Sb/Sn substitutions were published; generally, *ZT*s are much lower in comparison with the (Ti,Zr,Hf)NiSn-system for 300 K as well as for 800 K.

At 800 K (Figure 14), almost all *ZT*s are lower than 0.7 and also ZT_{max} rarely exceeds 1. He et al. [141] reached *ZT* > 1 for $Zr_{0.5}Hf_{0.5}Co_{0.9}Ni_{0.1}Sb$ at 1073 K, Liu et al. [158] acquired *ZT*s of almost 1 and around 1 for the series $(Zr_{1-x}Hf_x)_{0.88}Nb_{0.12}CoSb$. Xia et al. [116,165] investigated $Nb_{1-x}CoSb$ and $Nb_{0.8}Co_{1-x}Ni_xSb$ with *ZT* = 0.8–0.9. Zhu et al. [187] obtained *ZT* = 0.85 at 800 K with a peak *ZT* = 1.04 at 972 K for $ZrCo_{0.9}Ni_{0.1}Bi_{0.85}Sb_{0.15}$.

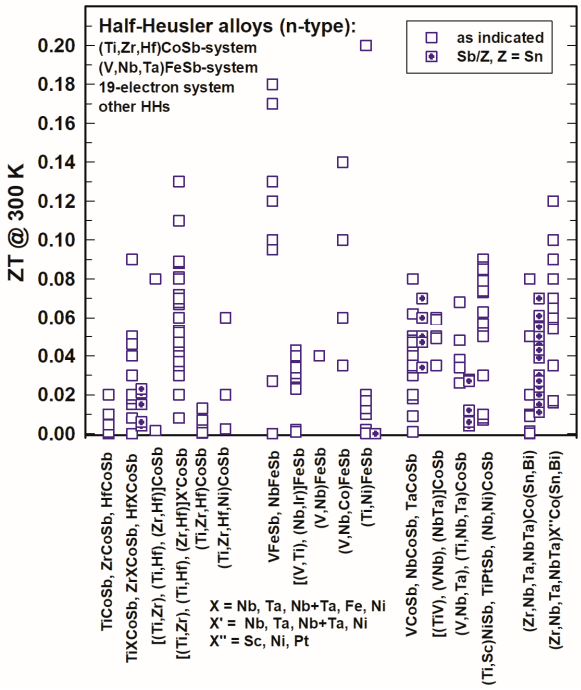

Figure 13. *ZT* at 300 K for the HH n-type (Ti,Zr,Hf)CoSb-system, (V,NbTa)FeSb-system, 19-electron system and other half-Heuslers.

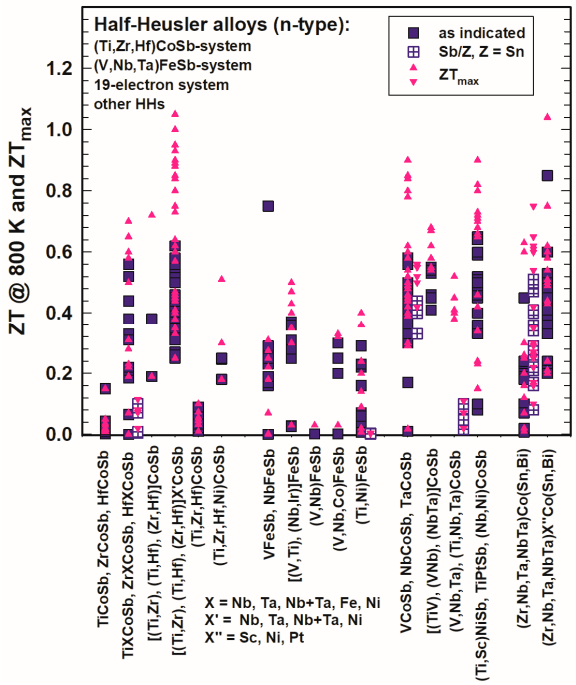

Figure 14. *ZT* at 800 K for the HH n-type (Ti,Zr,Hf)CoSb-system, (V,NbTa)FeSb-system, 19-electron system and other half-Heuslers.

3.3. P-Type Half-Heusler Alloys

All compounds with the respective references can be found in Table 2. In some cases, measurements were only performed below room temperature. Figures 15 and 16 represent the *ZT*s for p-type half-Heusler alloys at 300 K and 800 K as well as the peak *ZT*s, respectively.

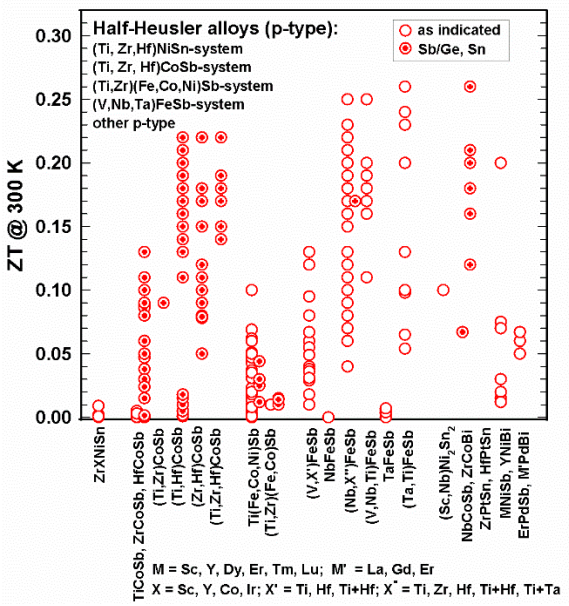

Figure 15. *ZT* at 300 K for the p-type HH alloys.

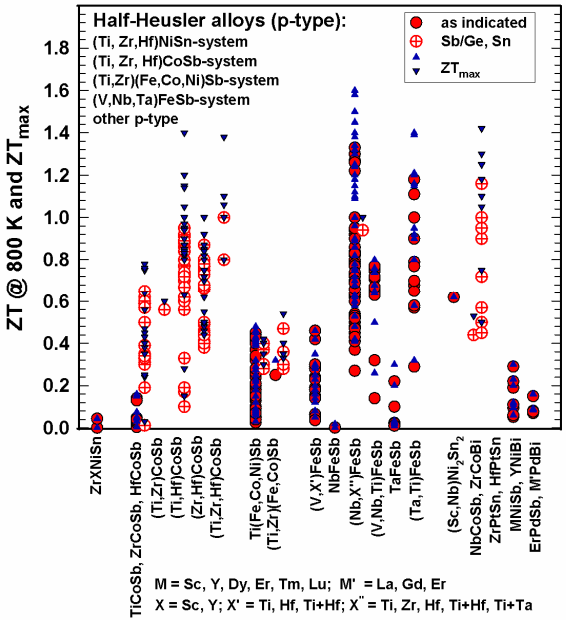

Figure 16. *ZT* at 800 K and ZT_{max} for the p-type HH alloys.

When looking at Section 3.3, it is obvious that many more n-type than p-type alloys were investigated. As depicted in Figure 15, at 300 K, all *ZT*s are below 0.3; at 800 K (Figure 16), most *ZT*s are lower than 1; however, several half-Heuslers in the (NbX″)FeSb series with X″ = Ti, Zr, Hf, Zr and Hf, as well as Ti + Ta, reach *ZT* = 1.4 at 800 K; the values for ZT_{max} in some cases reach or even exceed 1.4 and go up to 1.6.

It can be seen in Figures 15 and 16 that only data of two p-type compounds are available for the (Ti,Zr,Hf)NiSn-system, namely (Zr,Sc)NiSn [122] and (Zr,Y)NiSn [114] with rather low *ZT*s.

In the CoSb-based system, almost all compounds are substituted at the Sb-site by Sn, except for TiCoSb, which was also substituted by Ge [68]. Rausch et al. published in two separate works [120,121] rather high *ZT*s of the (Ti,Zr,Hf)$CoSb_{1-x}Sn_x$, series: the highest ZT_{max} = 1.4 for $Ti_{0.12}Zr_{0.44}Hf_{0.44}CoSb_{0.8}Sn_{0.2}$ at 963 K [121].

In the FeSb-based system, Yu et al. [150] achieved outstanding high peak *ZT* values (*ZT* = 1.2–1.6) for the series $Ti_{0.2}(Nb_{1-x}Ta_x)_{0.8}FeSb$; Zhu et al. gained *ZT*~1.4 at 1200 K for $Hf_{0.12}Nb_{0.88}FeSb$ [168] and for $Ti_{0.16}Ta_{0.84}FeSb$ [188].

Whereas many p-type half-Heuslers have *ZT*s < 1, the ZrCoBi-based half-Heuslers showed excellent thermoelectric performance, even more so for substituting at the Bi-site with *ZT* = 1.42 for $ZrCoBi_{0.65}Sb_{0.15}Sn_{0.20}$ at 973 K as reported by Zhu et al. [169].

Also, for p-type half-Heusler alloys, some research groups tried to enhance *ZT* via additions. Kimura et al. [71] added Co and Ir to ZrNiSn and converted this way the n-type to a p-type half-Heusler alloy; however, *ZT*s were rather low, i.e., below 0.3. Mallick et al. [159] investigated $(Hf_{0.7}Ti_{0.3}CoSb_{0.8}Sn_{0.2})_{1-x}(Cu_{1.98}Ni_{0.04}Te_{0.97}Se_{0.03})_x$: for x = 0.25 they could enhance *ZT* = 0.15 (without the chalcogenide) to *ZT* = 0.63 at 1023 K, which corresponds an enhancement of 320%. Hsu et al. [103] were successful in producing nanostructured HfO_2 during the ball-milling and spark–plasma–sintering process of $Zr_{0.5}Hf_{0.5}CoSb_{0.8}Sn_{0.2}$ and reached as highest *ZT* = 0.75. Xie et al. [193] enhanced *ZT* of Ti(Co,Fe)Sb with the addition of 1 atom percent nano inclusions of InSb by 450%; however, *ZT* = 0.33 is still very low.

Not only for n-type half-Heusler alloys, as described in Section 3.2.1, but also for the p-type, NbFeSb and $Ti_{0.15}Nb_{0.85}FeSb$, the influence of severe plastic deformation via high-pressure torsion was investigated by Rogl and colleagues [25,26]. For NbFeSb, the peak *ZT* could be enhanced by about 50% but is, with *ZT* = 0.00043, still very low. For $Ti_{0.15}Nb_{0.85}FeSb$, *ZT* was enhanced from *ZT* = 0.68 to *ZT* = 0.74 for the thermally stable sample.

Generally, for n- as well as for p-type half-Heuslers, most *ZT*s at 300 K are below 0.3. Above 300 K, many peak *ZT*s are below 1 but can reach 1.6. Whereas the most successful system for the n-type is the (Ti,Zr,Hf)NiSn-system with Sb/Sn substitution, for the p-type, it is the (V,Nb,Ta)FeSb-system doped with Ti, Zr or Hf.

3.4. Miscellaneous

On 8-electron half-Heusler alloys: Several authors have screened 8-electron half-Heusler alloys in DFT throughput calculations, identifying a series of compounds of interest in thermoelectrics. Vikram et al., in one publication [219], presented the TE properties of 21 half-Heusler alloys with a sum of 8 valence electrons (8-electron half-Heuslers); 6 of them showed *ZT*s between 0.8 and 1, such as LiSnAl, NaAlSn or LiAlGe. In another paper [220], he calculated the thermoelectric properties of a large number of ternary compounds of the type: group IA or IB element—group IIA or IIB element—group V element. From these results, he highlighted even *ZT*s such as *ZT* = 1.37 for RbPBa and *ZT* = 1.56 for AgPMg. Hoat et al. [221] also made theoretical investigations of the 8-electron half-Heusler alloy RbYSn, but they published only the power factors for the p- and n-types. So far, however, no experimental confirmation exists for the *ZT*s estimated from these DFT calculations.

On "double half-Heusler alloys", etc.: Some authors have coined the term "double half-Heusler alloys", "triple half-Heusler alloys", etc. These terms are not without problems. Firstly, double a half is full, but the authors certainly did not want to discuss full-Heusler alloys. Secondly, a formula such as $Ti_2FeCoSnSb$ from a structural chemical point of view indicates a fully ordered compound, where Fe,Co and Sn,Sb atoms fully occupy separate two-fold sites in a crystallographic subgroup of the space group of the half-Heusler phase. As such a subgroup cannot be found among the HH face-centered cubic space group type, the structure, therefore, needs to be transferred into a suitable body-centered tetragonal space group (cubic setting a,a,a needs to be transferred to a tetragonal cell: $a/\sqrt{2}, a/\sqrt{2}, a$) in order to find sites of two-fold multiplicity. Only if authors can prove the full atom order will the formula $Ti_2FeCoSnSb$ be proper. Similar arguments hold for "triple half-Heusler alloys", etc.

4. Conclusions

The review presented here attempts to cover all measured thermoelectric properties of p- and n-type half-Heusler alloys of the last 25 years. Of course, even with the best literature search, it may be possible to miss some publications. It also became obvious that there exist about twice as many papers of n-type than of p-type half-Heusler alloys.

As the figure of merit, *ZT* is dependent on three key figures, the electrical resistivity, the Seebeck coefficient and the thermal conductivity, the evaluations in this review, focusing on these key figures, may help to understand the interrelations between them as well as their influence on *ZT*.

It was found out that the n-type (Ti,Zr,Hf)NiSn-sytem generally has the highest *ZT*s and that (Ti,Zr)NiSn, (Ti,Hf)NiSn, (Zr,Hf)NiSn and especially (Ti,Zr,Hf)NiSn have higher *ZT*s than TiNiSn, ZrNiSn and HfNiSn. Furthermore, this investigation showed that doping, in most cases, does not enhance *ZT* as much as substituting at the antimony site, preferably tin by antimony. Various additions of nanoparticles could, in some cases, push up *ZT* slightly.

For the p-type, the (V,Nb,Ta)FeSb-system in respect of high *ZT* is the best and even better with compounds doped with Ti or Hf, but also quite remarkable *ZT*s were found for the (Ti,Zr,Hf)CoSb-system substituted by tin, and for ZrCoBi substituted at the bismuth site by antimony and tin.

All these evaluated *ZT*s are, of course, primarily dependent on the preparation method warranting a proper microstructure with small (preferably nano) grain size and a high density.

The present compilation may provide the data for the individual selection of p- and n-type leg materials suitable for an efficient thermoelectric generator within a given temperature gradient.

Author Contributions: Both authors (G.R. and P.F.R.) equally contributed to the manuscript. All authors have read and agreed to the published version of the manuscript.

Funding: This research received no external funding.

Data Availability Statement: The data sheet, which served as the basis for figures and tables, can be obtained from the authors upon reasonable request.

Conflicts of Interest: The authors declare no conflict of interest.

References

1. Poon, S.J. Electronic and thermoelectric properties of half-Heusler alloys. In *Semiconductors and Semimetals*; Elsevier: Amsterdam, The Netherlands, 2001; Volume 70, pp. 37–72.
2. Graf, T.; Felser, C.; Parker, S.S.P. Simple rules for the understanding of Heusler compounds. *Prog. Solid State Chem.* **2011**, *39*, 1–50. [CrossRef]
3. Lee, M.-S.; Poudeu, F.P.; Mahanti, S.D. Electronic structure and thermoelectric properties of Sb-based semiconducting half-Heusler compounds. *Phys. Rev. B* **2011**, *83*, 085204. [CrossRef]
4. Xie, W.; Weidenkaff, A.; Tang, X.; Zhang, Q.; Poon, J.; Tritt, T.M. Recent advances in nanostructured thermoelectric half-Heusler compounds. *Nanomaterials* **2012**, *2*, 379–412. [CrossRef] [PubMed]
5. Felser, C.; Hirohata, A. Heusler Alloys: Properties, Growth, Applications. In *Springer Series in Materials Science*; Springer: Cham, Switzerland, 2016; Volume 222, p. 2015945328.
6. Zhu, T.; Liu, Y.; Fu, C.; Heremans, J.P.; Snyder, J.G.; Zhao, X. Compromise and Synergy in High-Efficiency Thermoelectric Materials. *Adv. Mater.* **2017**, *20*, 1605884. [CrossRef] [PubMed]
7. Zhou, J.; Zhu, H.; Liu, T.-H.; Song, Q.; He, R.; Mao, J.; Liu, Z.; Ren, W.; Liao, B.; Singh, D.J.; et al. Large thermoelectric power factor from crystal symmetry-protected non-bonding orbital in half-Heuslers. *Nat. Commun.* **2018**, *9*, 1721–1730. [CrossRef]
8. Quinn, R.J.; Bos, J.-W.G. Advances in half-Heusler alloys for thermoelectric power generation. *Mater. Adv.* **2021**, *19*, 6246–6266. [CrossRef]
9. Freer, R.; Ekren, D.; Ghosh, T.; Biswas, K.; Qiu, P.; Wan, S.; Chen, L.; Han, S.; Fu, C.; Zhu, T.; et al. Key properties of inorganic thermoelectric materials—Tables. *J. Phys. Energy* **2022**, *4*, 022002. [CrossRef]
10. Hu, T.; Yang, D.; Su, X.; Yan, Y.; You, Y.; Liu, W.; Uher, C.; Tang, X. Interpreting the combustion process for high-performance ZrNiSn thermoelectric materials. *ACS Appl. Mater. Interfaces* **2018**, *10*, 864–872. [CrossRef]

11. Yu, C.; Zhu, T.-J.; Shi, R.-Z.; Zhang, Y.; Zhao, X.-B.; He, J. High-performance half-Heusler thermoelectric materials $Hf_{1-x}Zr_xNiSn_{1-y}Sb_y$ prepared by levitation melting and spark plasma sintering. *Acta Mater.* **2009**, *57*, 2757–2764. [CrossRef]
12. Yu, C.; Zhu, T.-J.; Xia, K.; Shen, J.J.; Yang, S.H.; Zhao, X. Reduced grain size and improved thermoelectric properties of melt spun (Hf, Zr) NiSn half-Heusler alloys. *J. Electron. Mater.* **2010**, *39*, 2008–2010. [CrossRef]
13. Karati, A.; Ghosh, S.; Mallik, R.C.; Shabadi, R.; Murty, B.S.; Varadaraju, U.V. Effect of processing routes on the microstructure and thermoelectric properties of half-Heusler $TiFe_{0.5}Ni_{0.5}Sb_{1-x}Sn_x$ (x = 0, 0.05, 0.1, 0.2) alloys. *J. Mater. Eng. Perform.* **2022**, *31*, 305–317. [CrossRef]
14. Bahrami, A.; Ying, P.; Wolff, U.; Perez-Rodriguez, N.; Schierning, G.; Nielsch, K.; He, R. Reduced lattice thermal conductivity for half-Heusler ZrNiSn through cryogenic mechanical alloying. *ACS Appl. Mater. Interfaces* **2021**, *13*, 38561–38568. [CrossRef] [PubMed]
15. Hasan, R.; Ur, S.-C. Thermoelectric and transport Properties of $V_{1-x}Ti_xFeSb$ half-Heusler system synthesized by controlled mechanical alloying process. *Electron. Mater. Lett.* **2018**, *14*, 725–732. [CrossRef]
16. He, R.; Zhu, T.; Ying, P.; Chen, J.; Giebeler, L.; Kühn, U.; Grossman, J.C.; Wang, Y.; Nielsch, K. High-pressure-sintering-induced microstructural engineering for an ultimate phonon scattering of thermoelectric half-Heusler compounds. *Small* **2021**, *17*, 2102045. [CrossRef] [PubMed]
17. Shen, Q.; Zhang, L.; Chen, L.; Goto, T.; Hirai, T. Thermoelectric properties of ZrNiSn-based half-Heusler compounds. *J. Mater. Sci. Lett.* **2001**, *20*, 2197–2199. [CrossRef]
18. Xing, Y.; Liu, R.; Liao, J.; Zhang, Q.; Xia, X.; Wang, C.; Huang, H.; Chu, J.; Gu, M.; Zhu, T.; et al. High-efficiency half-Heusler thermoelectric modules enabled by self-propagating synthesis and topologic structure optimization. *Energy Environ. Sci.* **2019**, *12*, 3390–3399. [CrossRef]
19. Xing, Y.F.; Liu, R.H.; Sun, Y.Y.; Chen, F.; Zhao, K.P.; Zhu, T.J.; Bai, S.Q.; Chen, L.D. Self-propagation high-temperature synthesis of half-Heusler thermoelectric materials: Reaction mechanism and applicability. *J. Mater. Chem. A* **2018**, *6*, 19470–19478. [CrossRef]
20. Hu, T.; Cao, W.; Yang, D.; Yan, Y.; Cao, Y.; Zhang, T.; Su, X.; Liu, W.; Poudeu-Poudeu, P.; Tang, X. Ultra-fast fabrication of bulk ZrNiSn thermoelectric material through self-propagating high-temperature synthesis combined with in-situ quick pressing. *Scripta Mater.* **2019**, *165*, 140–144. [CrossRef]
21. Birkel, C.S.; Zeier, W.G.; Douglas, J.E.; Lettiere, B.R.; Mills, C.E.; Seward, G.; Birkel, A.; Snedaker, M.L.; Zhang, Y.; Snyder, G.J.; et al. Rapid Microwave Preparation of Thermoelectric TiNiSn and TiCoSb half-Heusler Compounds. *Chem. Mater.* **2012**, *24*, 2558–2565. [CrossRef]
22. Birkel, C.S.; Douglas, J.E.; Lettiere, B.R.; Seward, G.; Verma, N.; Zhang, Y.; Pollock, T.M.; Seshadri, R.; Stucky, G.D. Improving the thermoelectric properties of half-Heusler TiNiSn through inclusion of a second full Heusler phase: Microwave preparation and spark plasma sintering of $TiNi_{1+x}Sn$. *Phys. Chem. Chem. Phys.* **2013**, *15*, 6990–6997. [CrossRef] [PubMed]
23. Lei, Y.; Li, Y.; Xu, L.; Yang, J.; Wan, R.; Long, H. Microwave synthesis and sintering of TiNiSn thermoelectric bulk. *J. Alloys Compd.* **2016**, *660*, 166–170. [CrossRef]
24. Lei, Y.; Cheng, C.; Li, Y.; Wan, R.; Mang, M. Microwave synthesis and enhancement of thermoelectric figure of merit in half-Heusler $TiNiSb_xSn_{1-x}$. *Ceram. Int.* **2017**, *43*, 9343–9347. [CrossRef]
25. Rogl, G.; Zehetbauer, M.J.; Rogl, P.F. The effect of severe plastic deformation on thermoelectric performance of skutterudites, half-Heuslers and Bi-tellurides. *Mater. Trans.* **2019**, *60*, 2071–2085. [CrossRef]
26. Rogl, G.; Ghosh, S.; Wang, L.; Bursik, J.; Grytsiv, A.; Mallik, R.C.; Chen, X.-Q.; Zehetbauer, M.; Rogl, P. Half-Heusler alloys: Enhancement of ZT after severe plastic deformation (ultra-low thermal conductivity). *Acta Mater.* **2020**, *183*, 285–300. [CrossRef]
27. Rogl, G.; Rogl, P.F. How severe plastic deformation changes the mechanical properties of thermoelectric skutterudites and half-Heusler alloys. *Front. Mater.* **2020**, *7*, 600261. [CrossRef]
28. Kim, H.-S.; Gibbs, Z.M.; Tang, Y.; Wang, H.; Snyder, G.J. Characterization of Lorenz number with Seebeck coefficient measurement. *APL Mater.* **2015**, *3*, 041506. [CrossRef]
29. Browning, V.M.; Poon, S.J.; Tritt, T.M.; Pope, A.L.; Bhattacharya, S. Thermoelectric properties of the half-Heusler compound (Zr, Hf)(Ni, Pd) Sn. *Proc. MRS Fall* **1998**, *545*, 403. [CrossRef]
30. Cook, B.A.; Meisner, G.P.; Yang, J.; Uher, C. High temperature thermoelectric properties of MNiSn (M = Zr, Hf). In Proceedings of the Eighteenth International Conference on Thermoelectrics, Baltimore, MD, USA, 29 August 1999; pp. 64–67.
31. Hohl, H.; Ramirez, A.P.; Goldmann, C.; Ernst, G.; Wölfing, B.; Bucher, E. Efficient dopants for ZrNiSn-based thermoelectric materials. *J. Phys. Condens. Matter* **1999**, *11*, 1697–1709. [CrossRef]
32. Uher, C.; Yang, J.; Hu, S.; Morelli, D.T.; Meisner, G.P. Transport properties of pure and doped MNiSn, M = Zr, Hf. *Phys. Rev. B* **1999**, *59*, 8615–8621. [CrossRef]
33. Shen, Q.; Chen, L.; Goto, T.; Hirai, T.; Yang, J.; Meisner, G.P.; Uher, C. Effects of partial substitution of Ni by Pd on the thermoelectric properties of ZrNiSn based half-Heusler compounds. *Appl. Phys. Lett.* **2001**, *79*, 4165–4172. [CrossRef]
34. Katayama, T.; Kim, S.W.; Kimura, Y.; Mishima, Y. The effects of quaternary additions on thermoelectric properties of TiNiSn-based half-Heusler alloys. *J. Electron. Mater.* **2003**, *32*, 1160–1165. [CrossRef]
35. Huang, X.Y.; Xu, Z.; Chen, L.D. The thermoelectric performance of $ZrNiSn/ZrO_2$ composites. *Solid State Commun.* **2004**, *130*, 181–185. [CrossRef]
36. Katsuyama, S.; Matsushima, H.; Ito, M. Effect of substitution for Ni by Co and/or thermoelectric properties of half-Heusler ZrNiSn. *J. Alloys Compd.* **2004**, *385*, 232–237. [CrossRef]

37. Kawaharada, Y.; Uneda, H.; Muta, H.; Kurosaki, K.; Yamanaka, S. High temperature thermoelectric properties of NiZrSn half-Heusler compounds. *J. Alloys Compd.* **2004**, *364*, 59–63. [CrossRef]
38. Kawaharada, Y.; Kurosaki, K.; Muta, H.; Uno, M.; Yamanaka, S. High temperature thermoelectric properties of TiCoSb half-Heusler compounds. *J. Alloys Compd.* **2004**, *384*, 308–311. [CrossRef]
39. Kim, S.W.; Kimura, Y.; Mishima, Y. Enhancement of high temperature thermoelectric properties of intermetallic compounds based on a skutterudite $IrSb_3$ and a half-Heusler TiNiSb. *Sci. Technol. Adv. Mater.* **2004**, *5*, 485–489. [CrossRef]
40. Kurosaki, K.; Muta, H.; Yamanaka, S. Thermoelectric properties of titanium-based half-Heusler compounds. *J. Alloys Compd.* **2004**, *384*, 51–56. [CrossRef]
41. Kurosaki, K.; Maekawa, T.; Muta, H.; Yamanaka, S. Effect of spark plasma sintering temperature on thermoelectric properties of (Ti, Zr, Hf)NiSn half-Heusler compounds. *J. Alloys Compd.* **2005**, *397*, 296–299. [CrossRef]
42. Muta, H.; Yamaguchi, T.; Kurosaki, K.; Yamanaka, S. Thermoelectric properties of ZrNiSn based half-Heusler compounds. In Proceedings of the Twentyfourth International Conference on Thermoelectrics, Clemson, SC, USA, 19 August 2005; pp. 339–342.
43. Sakurada, S.; Shutoh, N. Effect of Ti substitution on the thermoelectric properties of (Zr,Hf)NiSn half-Heusler compounds. *Appl. Phys. Lett.* **2005**, *86*, 082105. [CrossRef]
44. Sekimoto, T.; Kurosaki, K.; Muta, H.; Yamanaka, S. Annealing effect on thermoelectric properties of TiCoSb half-Heusler compound. *J. Alloys Compd.* **2005**, *394*, 122–125. [CrossRef]
45. Sekimoto, T.; Kurosaki, K.; Muta, H.; Yamanaka, S. Thermoelectric properties of (Ti,Zr,Hf)CoSb type half-Heusler compounds. *Mater. Trans.* **2005**, *46*, 1481–1484. [CrossRef]
46. Sekimoto, T.; Kurosaki, K.; Muta, H.; Yamanaka, S. Thermoelectric and thermophysical properties of TiCoSb, ZrCoSb, HfCoSb prepared by SPS. In Proceedings of the Twentyfourth International Conference on Thermoelectrics, Clemson, SC, USA, 19 August 2005; pp. 335–339.
47. Sakurada, S.; Shutoh, N. Thermoelectric properties of the $Ti_x(Zr_{0.5}Hf_{0.5})_{1-x}NiSn$ half-Heusler compounds. *J. Alloys Compd.* **2005**, *389*, 204–208.
48. Zhou, M.; Feng, C.; Chen, L.; Huang, X. Effects of partial substitution of Co by Ni on the high-temperature thermoelectric properties of TiCoSb-based half-Heusler compounds. *J. Alloys Compd.* **2005**, *391*, 194–197. [CrossRef]
49. Chen, L.D.; Huang, X.Y.; Zhou, M.; Shi, X.; Zhang, W.B. The high temperature thermoelectric performances of $Zr_{0.5}Hf_{0.5}Ni_{0.8}Pd_{0.2}Sn_{0.99}S_{b0.01}$ alloy with nanophase inclusions. *J. Appl. Phys.* **2006**, *99*, 064305. [CrossRef]
50. Culp, S.R.; Poon, S.J.; Hickman, N.; Tritt, T.M.; Blumm, J. Effect of substitutions on the thermoelectric figure of merit of half-Heusler phases at 800 °C. *Appl. Phys. Lett.* **2006**, *88*, 042106. [CrossRef]
51. Kimura, Y.; Zama, A.; Mishima, Y. Thermoelectric properties of p-type half-Heusler compounds HfPtSn and ZrPtSn. In Proceedings of the Twentyfifth International Conference on Thermoelectrics, Vienna, Austria, 6 August 2006; pp. 115–119.
52. Ono, Y.; Inayama, S.; Adachi, H.; Kajitani, T. Thermoelectric properties of doped half-Heuslers $NbCoSn_{1-x}Sb_x$ and $Nb_{0.99}Ti_{0.01}CoSn_{1-x}Sb_x$. *JPN J. Appl. Phys.* **2006**, *45*, 8740–8743. [CrossRef]
53. Sekimoto, T.; Kurosaki, K.; Muta, H.; Yamanaka, S. Thermoelectric and thermophysical properties of ErPdX (X = Sb and Bi) half-Heusler compounds. *J. Appl. Phys.* **2006**, *99*, 103701. [CrossRef]
54. Sekimoto, T.; Kurosaki, K.; Muta, H.; Yamanaka, S. Thermoelectric properties of $(Ti,Zr)CoSn_xSb_{1-x}$ half-Heusler compounds. In Proceedings of the Twentyfifth International Conference on Thermoelectrics, Vienna, Austria, 6 August 2006; pp. 128–131.
55. Sekimoto, T.; Kurosaki, K.; Muta, H.; Yamanaka, S. Thermoelectric properties of Sn-doped TiCoSb half-Heusler compounds. *J. Alloys Compd.* **2006**, *407*, 326–329. [CrossRef]
56. Sekimoto, T.; Kurosaki, K.; Muta, H.; Yamanaka, S. Thermoelectric and thermophysical properties of TiCoSb-ZrCoSb-HfCoSb pseudo ternary system prepared by spark plasma sintering. *Mater. Trans.* **2006**, *47*, 1445–1448. [CrossRef]
57. Katsuyama, S.; Matsuo, R.; Ito, M. Thermoelectric properties of half-Heusler alloys $Zr_{1-x}Y_xNiSn_{1-y}Sb_y$. *J. Alloys Compd.* **2007**, *428*, 262–267. [CrossRef]
58. Kim, S.-W.; Kimura, Y.; Mishima, Y. High temperature thermoelectric properties of TiNiSn-based half-Heusler compounds. *Intermetallics* **2007**, *15*, 349–356. [CrossRef]
59. Sekimoto, T.; Kurosaki, K.; Muta, H.; Yamanaka, S. Thermoelectric properties of half-Heusler Type LaPdBi and GdPdBi. *Mater. Trans.* **2007**, *48*, 2079–2082. [CrossRef]
60. Sekimoto, T.; Kurosaki, K.; Muta, H.; Yamanaka, S. High-thermoelectric figure of merit realized in p-type half-Heusler compounds: $ZrCoSn_xSb_{1-x}$. *JPN J. Appl. Phys.* **2007**, *46*, L673–L675. [CrossRef]
61. Wu, T.; Jiang, W.; Li, X.; Zhou, Y.; Chen, L. Thermoelectric properties of p-type Fe-doped TiCoSb half-Heusler compounds. *J. Appl. Phys.* **2007**, *102*, 103705. [CrossRef]
62. Culp, R.S.; Simson, J.W.; Poon, S.J.; Ponnambalan, V.; Edwards, J.; Tritt, T.M. (Zr,Hf)Co(Sb,Sn) half-Heusler phases as high-temperature (>700 °C) p-type thermoelectric materials. *Appl. Phys. Lett.* **2008**, *93*, 022105. [CrossRef]
63. Kimura, Y.; Tamura, Y.; Kita, T. Thermoelectric properties of directionally solidified half-Heusler compound NbCoSn alloys. *Appl. Phys. Lett.* **2008**, *92*, 012105. [CrossRef]
64. Xie, W.; Jin, Q.; Tang, X. The preparation and thermoelectric properties of $Ti_{0.5}Zr_{0.25}Hf_{0.25}Co_{1-x}Ni_xSb$ half-Heusler compounds. *J. Appl. Phys.* **2008**, *103*, 043711. [CrossRef]
65. Kimura, Y.; Ueno, H.; Mishima, Y. Thermoelectric properties of directionally solidified half-Heusler $(Ma_{0.5}Mb_{0.5})NiSn$ (Ma, Mb = Hf, Zr, Ti) alloys. *J. Electron. Mater.* **2009**, *38*, 934–939. [CrossRef]

66. Muta, H.; Kanemitsu, T.; Kurosaki, K.; Yamanaka, S. High-temperature thermoelectric properties of Nb-doped MNiSn (M = Ti, Zr) half-Heusler compound. *J. Alloys Compd.* **2009**, *469*, 50–55. [CrossRef]
67. Qiu, P.; Huang, X.; Chen, X.; Chen, L. Enhanced thermoelectric performance by the combination of alloying and doping in TiCoSb-based half-Heusler compounds. *J. Appl. Phys.* **2009**, *106*, 103703. [CrossRef]
68. Wu, T.; Jiang, W.; Li, X.; Bai, S.; Liufu, S.; Chen, L. Effects of Ge doping on the thermoelectric properties of TiCoSb-based p-type half-Heusler compounds. *J. Alloys Compd.* **2009**, *467*, 590–594. [CrossRef]
69. Kenjo, T.; Kimura, Y.; Mishima, Y. Phase stability and thermoelectric properties of half-Heusler compounds (Ti,M)NiSn (M = Zr, Hf). *Mater. Res. Soc. Symp. Proc.* **2010**, *1218*, 43–48. [CrossRef]
70. Kim, I.-H.; Kwon, J.-C.; Lee, Y.-G.; Yoon, M.-S.; Ryu, S.-L.; Kim, W.-G.; Ur, S.-C. Synthesis and thermoelectric properties of half-Heusler Zr-Ni-Sn alloy processed by mechanically alloying and hot-pressing. In *Materials Science Forum*; Trans Tech Publications Ltd.: Stafa-Zurich, Switzerland, 2010; Volume 658, pp. 33–36.
71. Kimura, Y.; Tanoguchi, T.; Kita, T. Vacancy site occupation by Co and Ir in half-Heusler ZrNiSn and conversion of the thermoelectric properties from n-type to p-type. *Acta Mater.* **2010**, *58*, 4354–4361. [CrossRef]
72. Ouardi, S.; Fecher, G.H.; Balke, B.; Kozina, X.; Stryganyuk, G.; Felser, C. Electronic transport properties of electron- and hole-doped semiconducting $C1_b$Heusler compounds: $NiTi_{1-x}M_xSn$ (M = Sc, V). *Phys. Rev. B* **2010**, *82*, 085108. [CrossRef]
73. Zhu, T.J.; Xiao, K.; Yu, C.; Shen, J.J.; Yang, S.H.; Zhou, A.J.; Zhao, X.B.; He, J. Effect of yttrium doping on the thermoelectric properties of $Hf_{0.6}Zr_{0.4}NiSn_{0.98}Sb_{0.02}$ half-Heusler alloys. *J. Appl. Phys.* **2010**, *108*, 044903. [CrossRef]
74. Zou, M.; Li, J.F.; Guo, P.; Kita, T. Synthesis and thermoelectric properties of fine-grained VFeSb system half-Heusler compound polycrystals with high phase purity. *J. Phys. D Appl. Phys.* **2010**, *43*, 415403. [CrossRef]
75. Gelbstein, Y.; Tal, N.; Yarmek, A.; Rosenberg, Y.; Dariel, M.P.; Ouardi, S.; Balke, B.; Felser, C.; Köhne, M. Thermoelectric properties of spark plasma sintered composites based on TiNiSn half-Heusler alloys. *J. Mater. Res.* **2011**, *26*, 1919–1924. [CrossRef]
76. Joshi, G.; Yan, X.; Wang, H.; Liu, W.; Chen, G.; Ren, Z. Enhancement in thermoelectric figure-of-merit of an n-type half-Heusler compound by the nanocomposite approach. *Adv. Energy Mater.* **2011**, *1*, 643–647. [CrossRef]
77. Makongo, J.P.A.; Misra, D.K.; Zhou, X.Y.; Pant, A.; Shabetai, M.R.; Su, X.L.; Uher, C.; Stokes, K.L.; Poudeu, P.F.P. Simultaneous large enhancements in thermopower and electrical conductivity of bulk nanostructured half-Heusler alloys. *J. Am. Chem. Soc.* **2011**, *133*, 18843–18852. [CrossRef]
78. Makongo, J.P.A.; Misra, D.K.; Salvador, J.R.; Takas, N.J.; Wang, G.; Shabetai, M.R.; Pant, A.; Poudel, P.; Uher, C.; Stokes, K.L.; et al. Thermal and electronic charge transport in bulk nanostructured $Zr_{0.25}Hf_{0.75}NiSn$ composites with full Heusler inclusions. *J. Solid State Chem.* **2011**, *184*, 2948–2960. [CrossRef]
79. Poon, S.J.; Wu, D.; Zhu, S.; Xie, W.; Tritt, T.M.; Venkatasubramanian, P.T.; Venkatasubramanian, R. Half-Heusler phases and nanocomposites as emerging high-ZT thermoelectric materials. *J. Mater. Res.* **2011**, *26*, 2795–2802. [CrossRef]
80. Schwall, M.; Balke, B. Niobium substitution in $Zr_{0.5}Hf_{0.5}NiSn$ based Heusler compounds for high power factors. *Appl. Phys. Lett.* **2011**, *98*, 042106. [CrossRef]
81. Simonson, J.W.; Wu, D.; Xie, W.J.; Tritt, T.M.; Poon, S.J. Introduction of resonant states and enhancement of thermoelectric properties in half-Heusler alloys. *Phys. Rev. B* **2011**, *83*, 235211. [CrossRef]
82. Yan, X.; Joshi, G.; Liu, W.; Lan, Y.; Wang, H.; Lee, S.; Simonson, J.W.; Poon, S.J.; Tritt, T.M. Enhanced thermoelectric figure of merit of p-type half-Heuslers. *Nano Lett.* **2011**, *11*, 556–560. [CrossRef] [PubMed]
83. Douglas, J.E.; Birkel, C.S.; Miao, M.-S.; Torbet, C.J.; Stucky, G.D.; Pollock, T.M.; Seshadri, R. Enhanced thermoelectric properties of bulk TiNiSn via formation of a $TiNi_2Sn$ second phase. *Appl. Phys. Lett.* **2012**, *101*, 183902. [CrossRef]
84. Populoh, S.; Aguirre, M.H.; Brunko, O.C.; Galazka, K.; Lu, Y.; Weidenkaff, A. High figure of merit in (Ti,Zr,Hf)NiSn half-Heusler alloys. *Scripta Mater.* **2012**, *66*, 1073–1107. [CrossRef]
85. Xie, H.-H.; Mi, J.-L.; Hu, L.-P.; Lock, N.; Chirstensen, M.; Fu, C.-G.; Brummerstedt Iversen, B.; Zhao, X.-B.; Zhu, T.-J. Interrelation between atomic switching disorder and thermoelectric properties of ZrNiSn half-Heusler compounds. *CrystEngComm* **2014**, *14*, 4467–4471. [CrossRef]
86. Yan, X.; Liu, W.; Wang, H.; Chen, S.; Shiomi, J.; Esfarjani, K.; Wang, H.; Wang, D.; Chen, G.; Ren, Z. Stronger phonon scattering by larger differences in atomic mass and size in p-type half-Heuslers $Hf_{1-x}Ti_xCoSb_{0.8}Sn_{0.2}$. *Energy Environ. Sci.* **2012**, *5*, 7543–7548. [CrossRef]
87. Appel, O.; Schwall, M.; Mogilyansky, D.; Köhne, M.; Balke, B.; Gelbstein, Y. Effects of microstructural evolution on the thermoelectric properties of spark-plasma-sintered $Ti_{0.3}Zr_{0.35}Hf_{0.35}NiSn$ half-Heusler compound. *J. Electron. Mater.* **2013**, *42*, 1340–1345. [CrossRef]
88. Birkel, C.S.; Douglas, J.E.; Lettiere, B.R.; Seward, G.; Zhang, Y.; Pollock, T.M.; Seshadri, R.; Stucky, G.D. Influence of Ni nanoparticle addition and spark plasma sintering on the TiNiSn-Ni system: Structure, microstructure, and thermoelectric properties. *Solid States Sci.* **2013**, *26*, 16–22. [CrossRef]
89. Chen, S.; Lukas, K.C.; Liu, W.; Opeil, C.P.; Chen, G.; Ren, Z. Effect of Hf concentration on thermoelectric properties of nanostructured n-type half-Heusler materials $Hf_xZr_{1-x}NiSn_{0.99}Sb_{0.01}$. *Adv. Energy Mater.* **2013**, *3*, 1210–1214. [CrossRef]
90. Downie, R.A.; MacLaren, D.A.; Smith, R.I.; Bos, J.W.G. Enhanced thermoelectric performance in TiNiSn-based half-Heuslers. *Chem. Commun.* **2013**, *49*, 4184–4186. [CrossRef] [PubMed]
91. Fu, C.; Xie, H.; Liu, Y.; Zhu, T.; Xie, J.; Zhao, X.B. Thermoelectric properties of FeVSb half-Heusler compounds by levitation melting and spark plasma sintering. *Intermetallics* **2013**, *32*, 39–43. [CrossRef]

92. Fu, C.; Liu, Y.; Xie, H.; Liu, X.; Zhao, X.; Snyder, J.G.; Xie, J.; Zhu, T. Electron and phonon transport in Co-doped $FeV_{0.6}Nb_{0.4}Sb$ half-Heusler thermoelectric materials. *J. Appl. Phys.* **2013**, *114*, 134905. [CrossRef]
93. Schwall, M.; Balke, B. Phase separation as a key to a thermoelectric high efficiency. *Phys. Chem. Chem. Phys.* **2013**, *15*, 1868–1872. [CrossRef]
94. Xie, W.J.; Yan, Y.G.; Zhu, S.; Zhou, M.; Populoh, S.; Galazka, K.; Poon, S.J.; Weidenkaff, A.; He, J.; Tang, X.F.; et al. Significant ZT enhancement in p-type Ti(Co,Fe)Sb-InSb nanocomposites via a synergistic high-mobility electron injection, energy-filtering and boundary-scattering approach. *Acta Mater.* **2013**, *61*, 2087–2094. [CrossRef]
95. Xie, W.J.; Wang, H.; Pei, Y.; Fu, C.; Liu, X.; Snyder, J.G.; Zhao, X.; Zhu, T. Beneficial contribution of alloy disorder to electron and phonon transport in half-Heusler thermoelectric materials. *Adv. Funct. Mater.* **2013**, *23*, 5123–5130. [CrossRef]
96. Yan, X.; Liu, W.; Chen, S.; Wan, H.; Zhang, Q.; Chen, G.; Ren, Z. Thermoelectric property study of nanostructured p-type half-Heuslers (Hf,Zr,Ti)$CoSb_{0.8}Sn_{0.2}$. *Adv. Energy Mater.* **2013**, *3*, 1195–1200. [CrossRef]
97. Zou, M.; Li, J.F.; Kita, T. Thermoelectric properties of fine-grained FeVSb half-Heusler alloys tuned to p-type by substituting vanadium with titanium. *J. Solid State Chem.* **2013**, *198*, 125–130. [CrossRef]
98. Bartholome, K.; Balke, B.; Zuckermann, D.; Köhne, M.; Müller, M.; Tarantik, K.; König, J. Thermoelectric modules based on half-Heusler materials produced in large quantities. *J. Electron. Mater.* **2014**, *43*, 1775–1781. [CrossRef]
99. Downie, R.A.; Mac Laren, D.A.; Bos, J.-W.G. Thermoelectric performance of multiphase XNiSn (X = Ti, Zr, Hf) half-Heusler alloys. *J. Mater. Chem. A* **2014**, *2*, 6107–6114. [CrossRef]
100. Downie, R.A.; Popuri, S.R.; Ning, H.; Reece, M.J.; Bos, J.-W.G. Effect of spark plasma sintering on the structure and properties of $Ti_{1-x}Zr_xNiSn$ half-Heusler alloys. *Materials* **2014**, *7*, 7094–7104. [CrossRef] [PubMed]
101. Fu, C.; Zhu, T.; Pei, Y.; Xie, H.; Wang, H.; Snyder, G.J.; Liu, Y.; Liu, Y.; Zhao, X. High band degeneracy contributes to high thermoelectric performance in p-type half-Heusler compounds. *Adv. Energy Mater.* **2014**, *4*, 1400600. [CrossRef]
102. Gazka, K.; Populoh, S.; Xie, W.; Yoon, S.; Saucke, G.; Hulliger, J.; Weidenkaff, A. Improved thermoelectric performance of $(Zr_{0.3}Hf_{0.7})NiSn$ half-Heusler compounds by Ta substitution. *J. Appl. Phys.* **2014**, *115*, 183704. [CrossRef]
103. Hsu, C.-C.; Liu, Y.-N.; Ma, H.-K. Effect of the $Zr_{0.5}Hf_{0.5}CoSb_{1-x}Sn_x/HfO_2$ half-Heusler nanocomposites on the ZT value. *J. Alloys Compd.* **2014**, *597*, 217–222. [CrossRef]
104. Joshi, G.; He, R.; Engber, M.; Samsonidze, G.; Pantha, T.; Dahal, E.; Dahal, K.; Yang, J.; Lan, Y.; Kozinsky, B.; et al. NbFeSb-based p-type half-Heuslers for power generation applications. *Energy Environ. Sci.* **2014**, *7*, 4070–4076. [CrossRef]
105. Krez, J.; Schmitt, J.; Snyder, G.J.; Felser, C.; Hermes, W.; Schwind, M. Optimization of the carrier concentration in phase-separated half-Heusler compounds. *J. Mater. Chem. A* **2014**, *2*, 13513–13518. [CrossRef]
106. Misra, D.K.; Bhardwaj, A.; Singh, S. Enhanced thermoelectric performance of a new half-Heusler derivative $Zr_9Ni_7Sn_8$ bulk nanocomposite: Enhanced electrical conductivity and low thermal conductivity. *J. Mater. Chem. A* **2014**, *2*, 11913–11921. [CrossRef]
107. Rausch, E.; Balke, B.; Ouardi, S.; Felser, C. Enhanced thermoelectric performance in the p-type half-Heusler (Ti,Zr,Hf)$CoSb_{0.8}Sn_{0.2}$ system via phase separation. *Phys. Chem. Chem. Phys.* **2014**, *16*, 25258–25262. [CrossRef] [PubMed]
108. Akram, R.; Zhang, Q.; Yang, D.; Zheng, Y.; Yan, Y.; Su, X.; Tang, X. Enhanced thermoelectric properties of La-doped ZrNiSn half-Heusler compound. *J. Electron. Mater.* **2015**, *44*, 3563–3570. [CrossRef]
109. Appel, O.; Zilber, T.; Kalabukhov, S.; Beerib, O.; Gelbstein, Y. Morphological effects on the thermoelectric properties of $Ti_{0.3}Zr_{0.35}Hf_{0.35}Ni_{1+\delta}Sn$ alloys following phase separation. *J. Mater. Chem. C* **2015**, *3*, 11653–11659. [CrossRef]
110. Chai, Y.W.; Oniki, T.; Kimura, Y. Microstructure and thermoelectric properties of a $ZrNi_{1.1}Sn$ half-Heusler alloy. *Acta Mater.* **2015**, *85*, 290–300. [CrossRef]
111. Chen, L.; Gao, S.; Zeng, X.; Mehdizadeh Dehkordi, A.; Tritt, T.M.; Poon, S.J. Uncovering high thermoelectric figure of merit in (Hf,Zr)NiSn half-Heusler alloys. *Appl. Phys. Lett.* **2015**, *107*, 041902. [CrossRef]
112. Fu, C.; Zhu, T.; Liu, Y.; Xie, H.; Zhao, X. Band engineering of high-performance p-type FeNbSb based half-Heusler thermoelectric materials for figure of merit $ZT > 1$. *Energy Environ. Sci.* **2015**, *8*, 216–220. [CrossRef]
113. Fu, C.; Bai, S.; Liu, Y.; Tang, Y.; Chen, L.; Zhao, X.; Zhu, T. Realizing high figure of merit in heavy-band p-type half-Heusler thermoelectric materials. *Nat. Commun.* **2015**, *6*, 8144–8151. [CrossRef] [PubMed]
114. Hattori, K.; Miyazaki, H.; Yoshida, K.; Inukai, M.; Nishino, Y. Direct observation of the electronic structure in thermoelectric half-Heusler alloys $Zr_{1-x}M_xNiSn$ (M = Y and Nb). *J. Appl. Phys.* **2015**, *117*, 205102. [CrossRef]
115. He, R.; Kim, H.S.; Lan, Y.; Wang, D.; Chen, S.; Ren, Z. Investigating the thermoelectric properties of p-type half-Heusler $Hf_x(Zr,Ti)_{1-x}CoSb_{0.8}Sn_{0.2}$ by reducing Hf concentration for power generation. *RSC Adv.* **2015**, *4*, 64711–64716. [CrossRef]
116. Huang, L.; He, R.; Chen, S.; Zhang, H.; Dahal, K.; Zhou, H.; Wang, H.; Zhang, Q.; Ren, Z. A new n-type half-Heusler thermoelectric material NbCoSb. *Mater. Res. Bull.* **2015**, *70*, 773–778. [CrossRef]
117. Huang, L.; Wang, Y.; Shuai, J.; Zhang, H.; Yang, S.; Zhang, Q.; Ren, Z. Thermal conductivity reduction by isoelectronic elements V and Ta for partial substitution of Nb in half-Heusler $Nb_{(1-x)/2}V_{(1-x)/2}Ta_xCoSb$. *RSC Adv.* **2015**, *5*, 102469–102476. [CrossRef]
118. Li, S.; Zhao, H.; Li, D.; Jin, S.; Gu, L. Synthesis and thermoelectric properties of half-Heusler alloy YNiBi. *J. Appl. Phys.* **2015**, *117*, 205101–205108. [CrossRef]
119. Liu, Y.; Xie, H.; Fu, C.; Snyder, G.J.; Zhao, X.; Zhu, T. Demonstration of a phonon-glass electron-crystal strategy in (Hf,Zr)NiSn half-Heusler thermoelectric materials by alloying. *J. Mater. Chem. A* **2015**, *3*, 22716–22722. [CrossRef]
120. Rausch, E.; Balke, B.; Stahlhofen, J.M.; Ouardi, S.; Burkhardt, U.; Felser, C. Fine tuning of thermoelectric performance in phase-separated half-Heusler compounds. *J. Mater. Chem. C* **2015**, *3*, 10409. [CrossRef]

121. Rausch, E.; Balke, B.; Ouardi, S.; Felser, C. Long-term stability of (Ti,Zr,Hf)$CoSb_{1-x}Sn_x$ thermoelectric p-type half-Heusler compounds upon thermal cycling. *Energy Technol.* **2015**, *3*, 1217–1224. [CrossRef]
122. Schmitt, J.; Gibbs, Z.M.; Snyder, G.J.; Felser, C. Resolving the true band gap of ZrNiSn half-Heusler thermoelectric materials. *Sci. Rep.* **2015**, *4*, 6888. [CrossRef]
123. Xie, H.; Wang, H.; Fu, C.; Liu, Y.; Snyder, G.J.; Zha, X.; Zhu, T. The intrinsic disorder related alloy scattering in ZrNiSn half-Heusler thermoelectric materials. *Nature Commun. Sci. Rep.* **2014**, *4*, 6888. [CrossRef]
124. Akram, R.; Yan, Y.; Yang, D.W.; She, X.Y.; Zheng, G.; Su, X.L.; Tang, X.F. Microstructure and thermoelectric properties of Sb doped $Hf_{0.25}Zr_{0.75}NiSn$ half-Heusler compounds with improved carrier mobility. *Intermetallics* **2016**, *74*, 1–7. [CrossRef]
125. Chai, Y.W.; Oniki, T.; Kenjo, T.; Kimura, Y. The effect of an isoelectronic Ti-Zr substitution on Heusler nanoprecipitation and the thermoelectric properties of a $(Ti_{0.2}Zr_{0.8})Ni_{1.1}Sn$ half-Heusler alloy. *J. Alloys Compd.* **2016**, *662*, 566–577. [CrossRef]
126. Chauhan, N.S.; Bhardwaj, A.; Senguttuvan, T.D.; Pant, R.P.; Mallik, R.C.; Misra, D.K. A synergistic combination of atomic scale structural engineering and panoscopic approach in p-type ZrCoSb-based half-Heusler thermoelectric materials for achieving high *ZT*. *J. Mater. Chem. C* **2016**, *4*, 5766–5778. [CrossRef]
127. Chen, L.; Zeng, X.; Tritt, T.M.; Poon, S.J. Half-Heusler alloys for efficient thermoelectric power conversion. *J. Electron. Mater.* **2016**, *45*, 5554–5556. [CrossRef]
128. Fu, C.; Wu, H.; Liu, Y.; He, J.; Zhao, X.; Zhu, T. Enhancing the figure of merit of heavy-band thermoelectric materials through hierarchical phonon scattering. *Adv. Sci.* **2016**, *3*, 1600035. [CrossRef]
129. Gürth, M.; Rogl, G.; Romaka, V.V.; Grytsiv, A.; Bauer, E.; Rogl, P. Thermoelectric high *ZT* half-Heusler alloys $Ti_{1-x-y}Zr_xHf_yNiSn$. *Acta Mater.* **2016**, *104*, 210–222. [CrossRef]
130. He, R.; Huang, L.; Wang, Y.; Samsonidze, G.; Kozinsky, B.; Zhang, Q.; Ren, Z. Enhanced thermoelectric properties of n-type NbCoSn half-Heusler by improving phase purity. *Appl. Mater.* **2016**, *4*, 104804. [CrossRef]
131. He, R.; Kraemer, D.; Mao, J.; Zeng, L.; Jie, Q.; Lan, Y.; Li, C.; Shuai, J.; Kim, H.S.; Liu, Y.; et al. Achieving high power factor and output power density in p-type half-Heuslers $Nb_{1-x}Ti_xFeSb$. *Proc. Natl. Acad. Soc. USA* **2016**, *113*, 13576–13581. [CrossRef]
132. Huang, L.; Zhang, Q.; Yuan, B.; Lai, X.; Yan, X.; Ren, Z. Recent progress in half-Heusler thermoelectric materials. *Mater. Res. Bull.* **2016**, *76*, 107–112. [CrossRef]
133. Liu, Y.; Makongo, J.P.A.; Page, A.; Sahoo, P.; Uher, C.; Stokes, K.; Poudeu, P.F.P. Distribution of impurity states and charge transport in $Zr_{0.25}Hf_{0.75}Ni_{1+x}Sn_{1-y}Sb_y$ nanocomposites. *J. Solid State Chem.* **2016**, *234*, 72–86. [CrossRef]
134. Rogl, G.; Grytsiv, A.; Gürth, M.; Tavassoli, A.; Ebner, C.; Wünschek, A.; Puchegger, S.; Soprunyuk, V.; Schranz, W.; Bauer, E.; et al. Mechanical properties of half-Heusler alloys. *Acta Mater.* **2016**, *107*, 178–195. [CrossRef]
135. Visconti, A.; Bernard-Granger, G.; Navone, C.; Leforestier, J.; Mingo, N. Microstructure investigations and thermoelectric properties of an n-type half-Heusler alloy sintered by spark plasma sintering. *Scripta Mater.* **2016**, *123*, 100–104. [CrossRef]
136. Zhang, H.; Wang, Y.; Huang, L.; Chen, S.; Dahal, H.; Wang, D.; Ren, Z. Synthesis and thermoelectric properties of n-type half-Heusler compound VCoSb with valence electron count of 19. *J. Alloys Compd.* **2016**, *654*, 321–326. [CrossRef]
137. Zhang, H.; Wang, Y.; Dahal, H.; Mao, J.; Huang, L.; Zhang, Q.; Ren, Z. Thermoelectric properties of n-type half-Heusler compounds $(Hf_{0.25}Zr_{0.75})_{1-x}Nb_xNiSn$. *Acta Mater.* **2016**, *113*, 41–47. [CrossRef]
138. Berry, T.; Ouardi, S.; Fecher, G.H.; Balke, B.; Kreiner, G.; Auffermann, G.; Schnelle, W.; Felser, C. Improving thermoelectric performance of TiNiSn by mixing MnNiSb in the half-Heusler structure. *Phys. Chem. Chem. Phys.* **2017**, *19*, 1543–1550. [CrossRef]
139. Berry, T.; Fu, C.; Auffermann, G.; Fecher, G.H.; Schnelle, W.; Serrano-Sanchez, F.; Yue, Y.; Liang, H.; Felser, C. Enhancing thermoelectric performance of TiNiSn half-Heusler compounds via modulation doping. *Chem. Mater.* **2017**, *29*, 7042–7048. [CrossRef]
140. Chen, L.; Liu, Y.; He, J.; Tritt, T.M.; Poon, S.J. High thermoelectric figure of merit by resonant dopant in half-Heusler alloys. *AIP Adv.* **2017**, *7*, 065208. [CrossRef]
141. He, R.; Zhu, H.; Sun, J.; Mao, J.; Reith, H.; Chen, S.; Schierning, G.; Nielsch, K.; Ren, Z. Improved thermoelectric performance of n-type half-Heusler $MCo_{1-x}Ni_xSb$ (M = Hf, Zr). *Mater. Today Phys.* **2017**, *1*, 24–30. [CrossRef]
142. Huang, L.; Zhang, Q.; Wang, Y.; He, R.; Shuai, J.; Zhang, J.; Wang, C.; Ren, Z. The effect of Sn doping on thermoelectric performance of n-type half-Heusler NbCoSb. *Phys. Chem. Chem. Phys.* **2017**, *19*, 25683–25690. [CrossRef]
143. Kim, K.S.; Kim, Y.M.; Mun, H.; Kim, J.; Park, J.; Borisevich, A.Y.; Lee, K.H.; Kim, S.W. Direct observation of inherent atomic-scale defect disorders responsible for high performance $Ti_{1-x}Hf_xNiSn_{1-y}Sb_y$ half-Heusler thermoelectric alloys. *Adv. Mater.* **2017**, *29*, 170209.
144. Lkhagvasuren, E.; Ouardi, S.; Fecher, G.H.; Auffermann, G.; Kreiner, G.; Schnelle, W.; Felser, C. Optimized thermoelectric performance of the n-type half-Heusler material TiNiSn by substitution and addition of Mn. *AIP Adv.* **2017**, *7*, 045010. [CrossRef]
145. Mao, J.; Zhou, J.; Zhu, H.; Liu, Z.; Zhang, H.; He, R.; Chen, G.; Ren, Z. Thermoelectric properties of n type ZrNiPb-based half-Heuslers. *Chem. Mater.* **2017**, *29*, 867–872. [CrossRef]
146. Rogl, G.; Sauerschnig, P.; Rykavets, Z.; Romaka, V.V.; Heinrich, P.; Hinterleitner, B.; Grytsiv, A.; Bauer, E.; Rogl, P. (V,Nb)-doped half Heusler alloys based on {Ti,Zr,Hf}NiSn with high *ZT*. *Acta Mater.* **2017**, *131*, 336–348. [CrossRef]
147. Silpawilawan, W.; Kurosaki, K.; Ohishi, Y.; Muta, H.; Yamanaka, S. FeNbSb p-type half-Heusler compound: Beneficial thermomechanical properties and high temperature stability for thermoelectrics. *J. Mater. Chem. C* **2017**, *5*, 6677–6681. [CrossRef]

148. Tavassoli, A.; Failamani, F.; Grytsiv, A.; Rogl, G.; Heinrich, P.; Müller, H.; Bauer, E.; Zehetbauer, M.; Rogl, P. On the half-Heusler compounds $Nb_{1-x}\{Ti,Zr,Hf\}_xFeSb$: Phase relations, thermoelectric properties at low and high temperature, and mechanical properties. *Acta Mater.* **2017**, *135*, 263–276. [CrossRef]
149. Visconti, A.; Navone, C.; Leforestier, J.; Mingo, N.; Bernard-Grange, G. Influence of the addition of HfO_2 particles on the thermoelectric properties of an n-type half-Heusler alloy sintered by spark plasma sintering. *J. Alloys Compds.* **2017**, *709*, 36–41. [CrossRef]
150. Yu, J.; Fu, C.; Liu, Y.; Xia, K.; Aydemir, U.; Chasapis, T.C.; Snyder, G.J.; Zhao, X.; Zhu, T. Unique role of refractory Ta alloying in enhancing the figure of merit of NbFeSb thermoelectric materials. *Adv. Energy Mater.* **2017**, *8*, 1701313. [CrossRef]
151. Zeier, W.G.; Anand, S.; Huang, L.; He, R.; Zhang, H.; Ren, Z.; Wolverton, C.; Snyder, G.J. Using the 18-electron rule to understand the nominal 19-electron half-Heusler NbCoSb with Nb vacancies. *Chem. Mater.* **2017**, *29*, 1210–1217. [CrossRef]
152. Barczak, S.A.; Halpin, J.E.; Buckman, J.; Decourt, R.; Pollet, M.; Smith, R.I.; MacLaren, D.A.; Bos, J.-W.G. Grain-by-grain compositional variations and interstitial metals—A new route toward achieving high performance in half-Heusler thermoelectrics. *ACS Appl. Mater. Interfaces* **2018**, *10*, 4786–4793. [CrossRef]
153. Chauhan, N.S.; Bathula, S.; Vishwakarma, A.; Bhardwaj, R.; Gahtori, B.; Srivastava, A.K.; Saravanan, M.; Dhar, A. A nanocomposite approach for enhancement of thermoelectric performance in hafnium-free half-Heuslers. *Materialia* **2018**, *1*, 168–174. [CrossRef]
154. Chauhan, N.S.; Bathula, S.; Vishwakarma, A.; Bhardwaj, R.; Johari, K.K.; Gahtori, B.; Saravanan, M.; Dhar, A. Compositional tuning of ZrNiSn half-Heusler alloys: Thermoelectric characteristics and performance analysis. *J. Phys. Chem. Solids* **2018**, *123*, 105–112. [CrossRef]
155. Chauhan, N.S.; Bathula, S.; Vishwakarma, A.; Bhardwaj, R.; Gahtori, B.; Kumar, A.; Dhar, A. Vanadium-doping-induced resonant energy levels for the enhancement of thermoelectric performance in Hf-free ZrNiSn half-Heusler alloys. *ACS Appl. Energy Mater.* **2018**, *1*, 757–764. [CrossRef]
156. Chauhan, N.S.; Bathula, S.; Vishwakarma, A.; Bhardwaj, R.; Johari, K.K.; Gahtori, B.; Dhar, A. Facile fabrication of p- and n-type half-Heusler alloys with enhanced thermoelectric performance and low specific contact resistance employing spark plasma sintering. *Mater. Lett.* **2018**, *228*, 250–253. [CrossRef]
157. Hu, C.; Xia, K.; Chen, X.; Zhao, X.; Zhu, T. Transport mechanisms and property optimization of p-type (Zr,Hf)CoSb half-Heusler thermoelectric materials. *Mater. Today Phys.* **2018**, *7*, 69–76. [CrossRef]
158. Liu, Y.; Fu, C.; Xia, K.; Chen, X.; Zhao, X.; Zhu, T. Lanthanide contraction as a design factor for high-performance half-Heusler thermoelectric materials. *Adv. Mater.* **2018**, *30*, 1800881. [CrossRef]
159. Mallick, M.M.; Vitt, S. Enhancing the thermoelectric performance of a p-type half-Heusler alloy, HfCoSb by incorporation of a band-matched chalcogenide, Cu_2Te. *J. Mater. Chem. A* **2018**, *6*, 14709–14716. [CrossRef]
160. Ren, W.; Zhu, H.; Zhu, Q.; Saparamadu, U.; He, R.; Liu, Z.; Mao, J.; Wang, C.; Nielsch, K.; Wang, Z.; et al. Ultrahigh power factor in thermoelectric system $Nb_{0.95}M_{0.05}FeSb$ (M = Hf, Zr, and Ti). *Adv. Sci.* **2018**, *5*, 1800278. [CrossRef]
161. Rogl, G.; Yubuta, K.; Romaka, V.V.; Michor, H.; Schafler, E.; Grytsiv, A.; Bauer, E.; Rogl, P. High-*ZT* half-Heusler thermoelectrics, $Ti_{0.5}Zr_{0.5}NiSn$ and $Ti_{0.5}Zr_{0.5}NiSn_{0.98}Sb_{0.02}$: Physical properties at low temperatures. *Acta Mater.* **2018**, *166*, 466–483. [CrossRef]
162. Shen, J.; Fu, C.; Liu, Y.; Zhao, X.; Zhu, T. Enhancing thermoelectric performance of FeNbSb half-Heusler compound by Hf-Ti dual doping. *Energy Storage Mater.* **2018**, *10*, 69–74. [CrossRef]
163. Silpawilawan, W.; Ohishi, Y.; Muta, H.; Yamanaka, S.; Kurosaki, K. Thermoelectric properties of p-type half-Heusler compounds $FeNb_{0.9}M_{0.1}Sb$ (M = Ti, Zr, Hf). *Mater. Trans.* **2018**, *59*, 1030–1034. [CrossRef]
164. Tavassoli, A.; Grytsiv, A.; Rogl, G.; Romaka, V.V.; Michor, H.; Reissner, M.; Bauer, E.; Zehetbauer, M.; Rogl, P. The half- Heusler system $Ti_{1+x}Fe_{1.33-x}Sb$—TiCoSb with Sb/Sn substitution: Phase relations, crystal structures and thermoelectric properties. *Dalton Trans.* **2018**, *47*, 879–897. [CrossRef] [PubMed]
165. Xia, K.; Liu, Y.; Anand, S.; Snyder, G.J.; Xin, J.; Yu, J.; Zhao, X.; Zhu, T. Enhanced thermoelectric performance in 18-electron $Nb_{0.8}CoSb$ half-Heusler compound with intrinsic Nb vacancies. *Adv. Funct. Mater.* **2018**, *28*, 1705845. [CrossRef]
166. Yan, Y.; Geng, W.; Qiu, J.; Ke, H.; Luo, C.; Yang, J.; Uher, C.; Tang, X. Thermoelectric properties of n-type ZrNiSn prepared by rapid non-equilibrium laser processing. *RSC Adv.* **2018**, *8*, 15796–15803. [CrossRef]
167. Zhao, D.; Zou, M.; Bo, L.; Wang, Y. Synthesis and thermoelectric properties of Pd-doped ZrCoBi half-Heusler compounds. *Materials* **2018**, *11*, 728–737. [CrossRef]
168. Zhu, T.; Fu, C.; Zhao, X. High figure of merit p-type FeNbHfSb thermoelectric material and the preparation method thereof. United States Patent US2018/0331268A1, 15 November 2018.
169. Zhu, H.; He, R.; Mao, J.; Zhu, Q.; Li, C.; Sun, J.; Ren, W.; Wang, Y.; Liu, Z.; Tang, Z.; et al. Discovery of ZrCoBi based half-Heuslers with high thermoelectric conversion efficiency. *Nat. Commun.* **2018**, *9*, 2497. [CrossRef]
170. Barczak, S.A.; Quinn, R.J.; Halpin, J.E.; Domosud, K.; Smith, R.I.; Baker, A.R.; Don, E.; Forbes, I.; Refson, K.; MacLaren, D.A.; et al. Suppression of thermal conductivity without impeding electron mobility in n-type XNiSn half-Heusler thermoelectrics. *J. Mater. Chem. A* **2019**, *7*, 27124–27134. [CrossRef]
171. Chauhan, N.S.; Bathula, S.; Gahtori, B.; Mahanti, S.D.; Bhattacharya, A.; Vishwakarma, A.; Bhardwaj, R.; Singh, V.N.; Dhar, A. Compositional tailoring for realizing high thermoelectric performance in hafnium-free n type ZrNiSn half-Heusler alloys. *ACS Appl. Mater. Interfaces* **2019**, *11*, 47830–47836. [CrossRef]

172. Du, N.V.; Rahman, J.U.; Meang, E.-J.; Lim, C.-H.; Shin, W.H.; Seo, W.-S.; Huy, P.T.; Kim, M.H.; Lee, S. Synthesis and thermoelectric properties of Ti-substituted $(Hf_{0.5}Zr_{0.5})_{1-x}Ti_xNiSn_{0.998}Sb_{0.002}$ half-Heusler compounds. *J. Alloys Compd.* **2019**, *773*, 1141–1145.
173. Ferluccio, D.A.; Halpin, J.E.; MacIntosh, K.L.; Quinn, R.J.; Don, E.; Smith, R.I.; MacLaren, D.A.; Bos, J.-W.G. Low thermal conductivity and promising thermoelectric performance in A_xCoSb (A = V, Nb or Ta) half-Heuslers with inherent vacancies. *J. Mater. Chem. C* **2019**, *7*, 6539–6547. [CrossRef]
174. Gong, B.; Li, Y.; Liu, F.; Zhu, J.; Wang, X.; Ao, W.; Zhang, C.; Li, J.; Xie, H.; Zhu, T. Continuously enhanced structural disorder to suppress the lattice thermal conductivity of ZrNiSn-based half-Heusler alloys by multielement and multisite alloying with very low Hf content. *ACS Appl. Mater. Interfaces* **2019**, *11*, 13397–13404. [CrossRef] [PubMed]
175. Grytsiv, A.; Romaka, V.V.; Watson, N.; Rogl, G.; Michor, H.; Hinterleitner, B.; Puchegger, S.; Bauer, E.; Rogl, P. Thermoelectric half-Heusler compounds TaFeSb and $Ta_{1-x}Ti_xFeSb$ ($0 \leq x \leq 0.11$): Formation and physical properties. *Intermetallics* **2019**, *111*, 106468. [CrossRef]
176. Huang, L.; Wang, J.; Mo, X.; Lei, X.; Ma, S.; Wang, C.; Zhang, Q. Improving the thermoelectric properties of the half-Heusler compound VCoSb by vanadium vacancy. *Materials* **2019**, *12*, 1637. [CrossRef]
177. Joshi, H.; Rai, D.P.; Hnamte, L.; Laref, A.; Thapa, R.K. A theoretical analysis of elastic and optical properties of half-Heusler MCoSb (M = Ti, Zr and Hf). *Heliyon* **2019**, *5*, e01155. [CrossRef]
178. Karati, A.; Mukherjee, S.; Mallik, R.C.; Shabadi, R.; Murty, B.S.; Varadaraju, U.V. Simultaneous increase in thermopower and electrical conductivity through Ta-doping and nanostructuring in half-Heusler TiNiSn alloys. *Materialia* **2019**, *7*, 100410. [CrossRef]
179. Karati, A.; Nagini, M.; Ghosh, S.; Shabadi, R.; Pradeep, K.G.; Mallik, R.C.; Murty, B.S.; Varadaraju, U.V. $Ti_2NiCoSnSb$—A new half-Heusler type high-entropy alloy showing simultaneous increase in Seebeck coefficient and electrical conductivity for thermoelectric applications. *Sci. Rep.* **2019**, *9*, 5331–5343. [CrossRef]
180. Li, S.; Zhu, H.; Mao, J.; Feng, Z.; Li, X.; Chen, C.; Cao, F.; Liu, X.; Singh, D.J.; Ren, Z.; et al. N-type TaCoSn-based half-Heuslers as promising thermoelectric materials. *ACS Appl. Mater. Interfaces* **2019**, *11*, 41321–41329. [CrossRef]
181. Mallik, M.M.; Rajput, K.; Vitta, S. Increasing figure-of-merit of ZrNiSn half-Heusler alloy by minimal substitution and thermal conductivity reduction. *J. Mater. Sci. Mater. Electron.* **2019**, *30*, 6139–6147. [CrossRef]
182. Qiu, Q.; Liu, Y.; Xia, K.; Fang, T.; Yu, J.; Zhao, X.; Zhu, T. Grain boundary scattering of charge transport in n-type (Hf,Zr)CoSb half-Heusler thermoelectric materials. *Adv. Energy Mater.* **2019**, *9*, 1803447. [CrossRef]
183. Shen, J.; Wang, Z.; Chu, J.; Bai, S.; Zha, X.; Chen, L.; Zhu, T. Low contact resistivity and interfacial behavior of p-type NbFeSb/Mo thermoelectric junction. *ACS Appl. Mater. Interfaces* **2019**, *11*, 14182–14190. [CrossRef] [PubMed]
184. Shen, J.; Fan, L.; Hu, C.; Zhu, T.; Xin, J.; Fu, T.; Zhao, D.; Zhao, X. Enhanced thermoelectric performance in the n-type NbFeSb half-Heusler compound with heavy element Ir doping. *Mater. Today Phys.* **2019**, *8*, 62–70. [CrossRef]
185. Synoradzki, K.; Ciesielski, K.; Veremchuk, I.; Borrmann, H.; Skokowski, P.; Szymanski, D.; Grin, Y.; Kaczorowski, D. Thermal and electronic transport properties of the half-Heusler phase ScNiSb. *Materials* **2019**, *12*, 1723–1734. [CrossRef] [PubMed]
186. Xia, K.; Nan, P.; Tan, S.; Wang, Y.; Ge, B.; Zhang, W.; Anand, S.; Zhao, X.; Snyder, G.J.; Zhu, T. Short-range order in defective half-Heusler thermoelectric crystals. *Energy Environ. Sci.* **2019**, *12*, 1568–1574. [CrossRef]
187. Zhu, H.; Mao, J.; Feng, Z.; Sun, J.; Zhu, Q.; Liu, Z.; Singh, D.J.; Wang, Y.; Ren, Z. Understanding the asymmetrical thermoelectric performance for discovering promising thermoelectric materials. *Sci. Adv.* **2019**, *5*, eaav5813. [CrossRef] [PubMed]
188. Zhu, H.; Mao, J.; Li, Y.; Sun, J.; Wang, Y.; Zhu, Q.; Li, G.; Song, Q.; Zhou, J.; Fu, Y.; et al. Discovery of TaFeSb-based half-Heuslers with high thermoelectric performance. *Nat. Commun.* **2019**, *10*, 270–278. [CrossRef]
189. Bae, W.; Hwang, J.Y.; Kim, S.-I.; Jeong, H.M.; Kim, S.; Lim, J.-H.; Kim, H.S.; Lee, K.H. Thermoelectric transport properties of n-Type Sb-doped (Hf,Zr,Ti)NiSn half-Heusler alloys prepared by temperature-regulated melt spinning and spark plasma sintering. *Appl. Sci.* **2020**, *10*, 4963–4970. [CrossRef]
190. Chauhan, N.S.; Raghuvanshi, P.R.; Tyagi, K.; Johari, K.K.; Tyagi, L.; Gahtori, B.; Bathula, S.; Bhattacharya, A.; Mahanti, S.D.; Singh, V.N.; et al. Defect engineering for enhancement of thermoelectric performance of (Zr,Hf)NiSn-based n-type half-Heusler alloys. *J. Phys. Chem. C* **2020**, *124*, 8584–8593. [CrossRef]
191. Ciesielski, K.; Synoradzki, K.; Veremchuk, I.; Skokowski, P.; Szymański, D.; Grin, Y.; Kaczorowski, D. Thermoelectric performance of the half-Heusler phases RNiSb (R = Sc, Dy, Er, Tm, Lu): High mobility ratio between majority and minority charge carriers. *Phys. Rev. Appl.* **2020**, *14*, 054046. [CrossRef]
192. El-Khouly, A.; Novitskii, A.; Adam, A.M.; Sedegov, A.; Kalugina, A.; Pankratova, D.; Karpenkov, D.; Khovaylo, V. Transport and thermoelectric properties of Hf-doped FeVSb half-Heusler alloys. *J. Alloys Compd.* **2020**, *820*, 153413. [CrossRef]
193. El-Khouly, A.; Novitskii, A.; Serhiienko, I.; Kalugina, A.; Sedegov, A.; Karpenkov, D.; Voronin, A.; Khovaylo, V.; Adam, A.M. Optimizing the thermoelectric performance of FeVSb half-Heusler compound via Hf-Ti double doping. *J. Power Sources* **2020**, *477*, 228768. [CrossRef]
194. Fang, T.; Xia, K.; Nan, P.; Ge, B.; Zhao, X.; Zhu, T. A new defective 19-electron TiPtSb half-Heusler thermoelectric compound with heavy band and low lattice thermal conductivity. *Mater. Today Phys.* **2020**, *13*, 100200. [CrossRef]
195. Graziosi, P.; Kumarasinghe, C.; Neophytou, N. Material descriptors for the discovery of efficient thermoelectrics. *ACS Appl. Energy Mater.* **2020**, *3*, 5913–5926. [CrossRef]
196. Johari, K.K.; Bhardwaj, R.; Chauhan, N.S.; Gahtori, B.; Bathula, S.; Auluck, S.; Dhakate, S.R. Band structure modification and mass fluctuation effects of isoelectronic germanium-doping on thermoelectric properties of ZrNiSn. *ACS Appl. Mater.* **2020**, *3*, 1349–1357. [CrossRef]

197. Kang, H.B.; Poudel, B.; Li, W.; Lee, H.; Saparamadu, U.; Nozariasbmarz, A.; Kang, M.G.; Gupta, A.; Heremans, J.; Priy, S. Decoupled phononic-electronic transport in multi-phase n-type half-Heusler nanocomposites enabling efficient high temperature power generation. *Mater. Today* **2020**, *36*, 63–72. [CrossRef]
198. Karati, A.; Hariharan, V.S.; Ghosh, S.; Prasad, A.; Nagini, M.; Guruvidyathri, K.; Mallik, R.C.; Shabadi, R.; Bichler, L.; Murty, B.S.; et al. Thermoelectric properties of half-Heusler high-entropy $Ti_2NiCoSn_{1-x}Sb_{1+x}$ (x = 0.5, 1) alloys with VEC > 18. *Scripta Mater.* **2020**, *186*, 375–380. [CrossRef]
199. Li, S.; Bai, F.; Wang, R.; Chen, C.; Li, X.; Cao, F.; Sui, J.; Liu, X.; Ren, Z.; Zhang, Q. Titanium doping to enhance thermoelectric performance of 19-electron VCoSb half-Heusler compounds with vanadium vacancies. *Ann. Phys.* **2020**, *525*, 1900440. [CrossRef]
200. Li, N.; Zhu, H.; He, W.; Zhang, B.; Cui, W.; Hu, Z.-Y.; Sang, X.; Lu, X.; Wang, G.; Zhou, X. Realizing both n- and p-types of high thermoelectric performance in Fe1-xNixTiSb half-Heusler compounds. *J. Mater. Chem. C* **2020**, *8*, 3156–3164. [CrossRef]
201. Pedersen, S.V.; Croteau, J.R.; Kempf, N.; Zhang, Y.; Butt, D.P.; Jaques, B.J. Novel synthesis and processing effects on the figure of merit for NbCoSn, NbFeSb, and ZrNiSn based half-Heusler thermoelectrics. *J. Solid State Chem.* **2020**, *285*, 121203. [CrossRef]
202. Serrano-Sanchez, F.; Luo, T.; Yu, J.; Xie, W.; Le, C.; Auffermann, G.; Weidenkaff, A.; Zhu, T.; Zhao, X.; Alonso, J.A.; et al. Thermoelectric properties of n-type half-Heusler NbCoSn with heavy-element Pt substitution. *J. Mater. Chem. A* **2020**, *8*, 14822–14828. [CrossRef]
203. Yang, X.; Jiang, Z.; Kang, H.; Chen, Z.; Guo, E.; Liu, D.; Yang, F.; Li, R.; Jiang, X.; Wang, T. Enhanced thermoelectric performance of $Zr_{1-x}Ta_xNiSn$ half-Heusler alloys by diagonal-rule doping. *ACS Appl. Mater. Interfaces* **2020**, *12*, 3773–3783. [CrossRef] [PubMed]
204. Yu, J.; Xing, Y.; Hu, C.; Huang, Z.; Qiu, Q.; Wang, C.; Xia, K.; Wang, Z.; Bai, S.; Zhao, X.; et al. Half-Heusler thermoelectric module with high conversion efficiency and high-power density. *Adv. Energy Mater.* **2020**, *10*, 2000888. [CrossRef]
205. Wang, R.-F.; Li, S.; Xue, W.-H.; Chen, C.; Wang, Y.-M.; Liu, X.-J.; Zhang, Q. Enhanced thermoelectric performance of n-type TiCoSb half- Heusler by Ta doping and Hf alloying. *Rare Met.* **2021**, *40*, 40–47. [CrossRef]
206. Zelenka, F.; Brož, P.; Vrestal, J.; Bursik, J.; Zemanova, A.; Rogl, G.; Rogl, P. Study of thermal stability of half-Heusler alloys $TiFe_{1.33}Sb$ and $Ti_xNb_{1-x}FeSb$ (x = 0, 0.15) by differential thermal analysis and Knudsen effusion method. *Calphad* **2021**, *74*, 102292. [CrossRef]
207. Guo, S.; Anad, S.; Brod, M.K.; Zhang, Y.; Snyder, G.J. Conduction band engineering of half-Heusler thermoelectrics using orbital chemistry. *J. Mater. Chem. A* **2022**, *10*, 3051. [CrossRef]
208. Karati, A.; Ghosh, S.; Nagini, M.; Mallik, R.C.; Shabadi, R.; Murty, B.S.; Varadaraju, U.V. Thermoelectric properties of nanocrystalline half-Heusler high-entropy $Ti_2NiCoSn_{1-x}Sb_{1+x}$(x = 0.3, 0.5, 0.7, 1) alloys with VEC > 18. *J. Alloys Compds.* **2022**, *927*, 166578. [CrossRef]
209. Karati, A.; Mishra, S.R.; Ghosh, S.; Mallik, R.C.; Shabadi, R.; Murty, B.S.; Ramanujan, R.V.; Yadav, S.K.; Murty, B.S.; Varadaraju, U.V. Thermoelectric properties of a high entropy half-Heusler alloy processed by a fast powder metallurgy route. *J. Alloys Compd.* **2022**, *924*, 166108. [CrossRef]
210. Mesaritis, G.; Ioannou, I.; Delimitis, A.; Hatzikraniotis, E.; Gelbstein, Y.; Kyratsi, T. n-type (Zr,Ti)NiSn half-Heusler materials via mechanical alloying: Structure, Sb-doping and thermoelectric properties. *J. Phys. Chem. Solids* **2022**, *167*, 110735. [CrossRef]
211. Serrano-Sanchez, F.; Yao, M.; He, B.; Chen, D.; Gloskovskii, A.; Fedorov, A.; Auffermann, G.; Liu, E.; Burkhardt, U.; Fecher, G.H.; et al. Electronic structure and low-temperature thermoelectric transport of TiCoSb single crystals. *Nanoscale* **2022**, *14*, 10067. [CrossRef]
212. Yang, X.; Wang, Y.; Min, R.; Chen, Z.; Guo, E.; Kang, H.; Li, L.; Jiang, X.; Wang, T. Enhancement in thermoelectric properties of ZrNiSn-based alloys by Ta-Hf Co-doping. *Acta Mater.* **2022**, *233*, 117976. [CrossRef]
213. Barczak, S.A.; Kennedy, B.F.; da Silva, I.; Bos, J.-W.G. Mechanistic insights into the formation of thermoelectric TiNiSn from in situ neutron powder diffraction. *Chem. Mater.* **2023**, *35*, 3694. [CrossRef] [PubMed]
214. Chen, R.; Yan, Y.; Zhang, W.; Liu, F.; Kang, H.; Guo, E.; Chen, Z.; Wang, T. Enhanced thermoelectric properties of $Zr_{0.85-x}Hf_xNb_{0.15-y}Ta_yCoSb$ medium-entropy alloys: Tradeoff between "What to Alloy" and "How Much to Alloy". *Chem. Mater.* **2023**, *35*, 2202. [CrossRef]
215. Ciesielski, K.; Synoradzki, K.; Szymański, D.; Tobita, K.; Berent, K.; Obstarczyk, P.; Kimura, K.; Kaczorowski, D. Half- Heusler phase TmNiSb under pressure: Intrinsic phase separation, thermoelectric performance and structural transition. *Sci. Rep.* **2023**, *13*, 1592. [CrossRef]
216. Liu, R.; Wang, C.; Huang, J.; Luo, P.; Liu, X.; Ye, S.; Dong, Z.; Zhang, J.; Luo, J. Preparation and thermoelectric properties of Sc-doped $Ti_{1-x}NiSb$ half-Heusler alloys. *Acta Phys. Sin.* **2013**, *72*, 20230035.
217. Min, R.; Gao, Y.; Jiang, X.; Yang, X.; Li, L.; Kang, H.; Guo, E.; Chen, Z.; Wang, T. Enhancement in the thermoelectric performance of ZrNiSn-based alloys through extra Zr-rich nanoprecipitates with superstructures. *Chem. Eng. J.* **2023**, *464*, 142531. [CrossRef]
218. Verma, A.K.; Johari, K.K.; Dubey, P.; Candolfi, C.; Lenoir, B.; Walia, S.; Dhakate, S.R.; Gahtori, B. Coupling of electronic transport and defect engineering substantially enhances the thermoelectric performance of p-type TiCoSb HH alloy. *J. Alloys Compds.* **2023**, *947*, 169416. [CrossRef]
219. Vikram, B.S.; Barman, C.K.; Alam, A. Accelerated discovery of new 8-electron half-Heusler compound as promising energy and topological quantum materials. *J. Phys. Chem. C* **2019**, *123*, 12. [CrossRef]

220. Vikram, B.S.; Kangsabanik, J.; Alam, A. Accurate high-throughput screening of I-II-V 8-electron half-Heusler compounds for renewable-energy application. *arXiv* **2019**, arXiv:1910.02984v1.
221. Hoat, D.M.; Naseri, M. Electronic and thermoelectric properties of RbYSn half-Heusler compound with a 8 valence electrons: Spin-orbit coupling effect. *Chem. Phys.* **2020**, *528*, 110510. [CrossRef]